FLUID EXCHANGE AND OXYGEN FLUX THROUGH SALMONID REDDS

R&D Technical Report W225

Paul Carling, Paul Taylor, Barry Hankin and Ian Benson

Research Contractors:

Department of Geography
Southampton University
and
Institute of Environmental & Natural Sciences
Lancaster University

Publishing Organisation
Environment Agency
Rio House
Waterside Drive
Aztec West
Almondsbury
Bristol BS32 4UD
Tel: 01454 624400 Fax: 01454 624409

 ISBN: 1844320626

Dissemination status
Internal: Released to Regions
External: Public Domain

Statement of Use
This report describes a study undertaken to improve our knowledge of the mechanisms involved in the flow of oxygenated water through salmonid redds. The study also recalibrated and tested the American SIDO software for potential use in predicting the likely impact of environmental change on UK salmonid populations. The report is for information and will be of interest to Agency Fisheries staff and others involved in the management of salmonid fisheries.

Research Contractor
This document was produced under R&D Project W2-022 by:

Depart. of Geography, and Southampton University, Southampton, SO17 1BJ,

Hydrodynamics & Sedimentology Laboratory, Institute of Environmental & Natural Sciences, Lancaster University, Lancaster, LA1 4YB.

Tel: 01524 593169
Fax: 01524 847099

Environment Agency Project Manager
The Environment Agency's Project Manager for R&D Project No W2-022 was Jonathan Shatwell, North West Region, Warrington.

Further copies of this report are available from:
Environment Agency R&D Dissemination Centre, c/o WRc, Frankland Road, Swindon, Wilts SN5 8YF

tel: 01793-865138 fax: 01793-514562 e-mail: publications@wrcplc.co.uk

CONTENTS

LIST OF FIGURES

LIST OF FIGURES (CONTINUED)

LIST OF FIGURES (CONTINUED)

Page

LIST OF TABLES

EXECUTIVE SUMMARY

- **Background**

Populations of indigenous salmonid fish within the UK include the Brown Trout (*Salmo trutta*) and the Atlantic Salmon (*Salmo salar*). These fish spawn in headwater streams burying their eggs in river gravels. The female fish digs a hollow in the gravel that is progressively backfilled as one or more pockets of eggs are buried. The cutting action of the female removes fine sediment from the gravel, which is washed away downstream. The final structure in the river bed is know as a 'redd', and consists of a hollow (the 'pot') immediately upstream of a raised elongate mound of gravel ('the tail') beneath which lie the fish eggs. Thus eggs are buried in clean gravel through which river water may percolate freely. This percolation, or intragravel flow, is important as the river water provides oxygen, necessary for development of the embryo, and also removes metabolic waste products from the vicinity of the egg pockets.

It has been argued that the shape of the redd induces an increased rate of flow through the gravel. In addition it is known that if fine sediment settles out from the river flow into the cleaned gravel then the pore spaces in the redd may be blocked. This clogging may reduce the intragravel flow such that the eggs are starved of oxygen and, in addition, the blocked pore space may prevent young fish from emerging at the riverbed surface after hatching. Thus siltation may reduce recruitment of young Salmon and Trout. Siltation is an environmental issue as it is often claimed that increased human disturbance and mismanagement of soils in river catchments is leading to erosion, higher suspended sediment loads in rivers and consequently greater rates of deposition of sediment in spawning beds. Enhanced siltation may cause salmonids to abandon traditional spawning areas. Alternatively excessive silt settling into the gravel after spawning clogs the pore space as described above.

Consequently, to manage and enhance salmonid spawning gravels, there is a need to understand the process by which the river flow patterns are modified by the shape of the redd so as to drive the intragravel flow past the egg pockets. The pathways and strength of the resultant intragravel flow need to be known if it is going to be possible to predict the supply of oxygenated water to fish eggs and thus predict the survival of eggs to hatching. Prediction is possible using software designed to predict the strength of flow through the redd. 'First-generation' software exists (the SIDO model) developed in the USA for application to North American fish, but this has not been widely tested in the USA nor has it been calibrated or tested for UK salmonids.

- **Objectives**

The aims of this study are to fully describe the nature of turbulent flow over an artificial redd built in gravel in an hydraulic flume. The study will identify the detail of the flow pattern around the redd and locate zones of high and low pressure at the gravel surface which promote intragravel flow. The main flow paths through the gravel will be delineated and the rate of intragravel flow will be determined at critical locations throughout the redd structure. The software SIDO will be recalibrated for

use with UK salmonid fishes and graphical output will be produced of the predicted changes within the redd environment of such parameters as dissolved oxygen, egg survival and fish emergence. In summary the aim is to fully understand the physical environment around a salmonid redd and to test the recalibrated software SIDO for potential use by agencies within the UK.

- **Results**

Earlier studies of flow over and through salmonid redds have been crude in execution. The results of the present study are extremely detailed, use state-of-the-art equipment and represent an internationally important definitive study of turbulent flow above a three-dimensional fish redd. The description of the turbulent flow is highly specialised and is reported fully in a M.Phil. thesis (Taylor, 2000). In this technical report simple graphical plots detail the complex flow structure over the redd, showing the effect of the topography on the flow patterns. Notably the 'pot' induces downward flow, both from above and from the sides, 'focussing' flow into the base of the downstream portion of the 'pot'. At this location the topography of the 'tail' is beginning to rise up into the river flow such that water pressure builds up just at the point where the concave slope coming up out of the 'pot' becomes convex in the upstream part of the 'tail'. In the 'pot' upstream and downward directed currents are also generated but these are quite weak and inconsequential compared to the flow moving into the pot and towards the tail.

The strong pressure gradient drives an intragravel current through the 'tail' just at that location where the egg pockets usually are to be found. In addition, on the downstream part of the tail the bed level is dropping away towards the flat bed level. This reduction in elevation causes the river flow to expand immediately downstream of the top of the 'tail' and causes a low-pressure area to develop above the gravel surface of the 'tail'. This low pressure induces up welling of intragravel flow and thus 'draws' the intragravel flow through the redd structure to the benefit of the egg pockets. Dye tracing shows the path of flow through the gravel and confirms that the main flow lines are driven by the high and low pressure regions on the bed. A novel tracing technique developed for this study also allows, for the first time, to quantify the rate of flow at different locations along these flow lines. This simple method has shown that the rate of flow, and hence the rate of oxygen supply, is greatest exactly at those locations wherein the egg pockets usually lie. This tracing method should be transferable to the field although at the time of writing no field trials have been conducted.

The SIDO model was recalibrated for the UK situation and three test scenarios developed for a reach of a major UK Salmon spawning river - the River Lune in North-west England. Graphical output demonstrates that the revised model, SIDO-UK, generally functions well. This means that the model usually predicts rational values for factors of interest in respect of UK salmonids. Where the model performs less well in determining absolute values, the trend and the magnitude are usually correct. Thus at this time the partially revised SIDO-UK can be used to demonstrate trends in factors highlighting reducing or improving environmental conditions. The greatest uncertainty exists in predicting the incubation period leading to hatching of eggs, and in determining percentage survival when fry emerge. For example the original SIDO uses an algorithm determining days to hatching (Chinook Salmon and

Steelhead Trout) as a function of dissolved oxygen (DO) content and water temperature. When an alternative function is used in SIDO-UK for Atlantic Salmon, using DO, temperature *and* a reduction in intragravel flow rate (for example induced by siltation) then the time to hatching increases markedly. SIDO-UK currently does not use a modified function to predict fry emergence; this is because there is little information on fry emergence for UK salmonids. Consequently functions developed for Chinook Salmon and Steelhead Trout are used whereby emergence is predicated upon the grainsize distribution of the whole redd. We used grainsize data for Atlantic Salmon in this function, but the function is crude and does not allow, for example, for surface sand seals that can develop entombing fry in otherwise clean gravel.

- **Recommendations**

SIDO-UK can be used in its present form to predict the likely impact of environmental change on UK salmonid populations. The addition of a function allowing for reduced intragravel flow rate means that the effect of siltation problems may be readily addressed. However we have no suitable test data to check the fry emergence predictions which consequently remain suspect. Thus the strengths and limitation of the SIDO-UK model are noted and recommendations are made in the text for further calibration and testing against field data. The latter data will need to be especially obtained from a range of UK rivers of strategic importance for salmonid recruitment. In addition, further laboratory tests are recommended wherein fine sediment is added to clean river gravel in an hydraulic flume. Such a procedure will simulate the siltation process that occurs in natural redds. The effect of intragravel flow rates can be monitored and SIDO-UK modified in the light of the field and laboratory findings. Outstanding biological issues are: the urgent need for a better understanding of egg physiology, particularly oxygen uptake under differing environmental conditions and the effect on embryo development. In addition better understanding is required of the controls mediating fry emergence.

KEYWORDS:

Atlantic Salmon; Brown Trout: Salmonid Fish; Salmon Spawning; Salmon Redds; Turbulent Flow; Intragravel Flow; Dissolved Oxygen; SIDO.

1 PROJECT DESCRIPTION

1.1 Introduction

Biodiversity is an important factor in the environmental sector. Preserving species in their natural habitat is a pressing need in ensuring the overall quality of river habitats. This report considers the UK Salmonid species: *Salmo salar* (Atlantic Salmon) and *Salmo trutta*, the latter in either its freshwater form (Brown Trout) or andronomous form (Sea Trout). Salmonids in particular are an important indicator of water quality, a locally important commercial or recreational fishery, and are often a tourist attraction. Decline in salmonid populations has been recorded over the past few decades (most easily recorded as a decline in the number of catches by anglers) and is a cause for concern amongst several interest groups such as anglers and environmental groups.

Theurer (1985) identifies three specific causes of the problem within freshwater habitats– degradation in habitat, poor fish passage measures (e.g. at dams) and over fishing. Chemical or physical pollution through the presence of fine suspended sediment is a particular problem in some rivers. Chemical alterations can damage the gills of fish, making respiration difficult. In extreme cases, fish can display burns, damaged eyes and sterility. Fine suspended sediment also can have unfortunate consequences directly causing abrasion of gills and scales, or anoxyia leading to stress, susceptibility to disease or morbidity. However, fine suspended sediments can be a particular problem during spawning when the fish excavates a 'nest' or 'redd' in river-bed gravel of a suitable composition. A build-up of fines in the redd can reduce the flow of oxygenated water through the gravel, depriving the fish eggs of vital oxygen. This technical report considers the nature of flow above the redd and the exchange of oxygenated water between the pore space within the gravel and the channel flow.

1.1.1 The spawning process

Cutting of the redd is accomplished by the female fish lying on her side and violently flexing her body in the vertical (Fig. 1.1). The resultant suction lifts particles from the bed which are then carried in a downstream direction by the stream current. This results in a hollow in the river bed. The female deposits one or more clump of eggs within the hollow and these eggs are then fertilised by the male. Although the current within the pot may disperse the eggs to some degree, usually 'pockets' of hundreds of eggs persist. As the female progressively excavates in an upstream direction the egg pockets are sequentially buried by the 'tailspill' which consists of coarser gravel which drops back to the bed within a few decimetres downstream. Finer sediment fractions (chiefly less than 1mm) may be disturbed and settle to the bottom of the excavation or, more usually, may be completely removed from the vicinity of the redd by transport in suspension within the flow. Thus the cutting action of the female not only buries the eggs but also causes the finer fractions to be removed from much of the gravel. When completed the redd typically consists of an upstream hollow or 'pot' where excavation finished with an adjacent mound of tailspill (the 'tail') downstream. Most salmonid redds contain at least two egg pockets located in the upstream portion of the tail.

Thus the egg pockets should lie within gravel with a significant reduction in the percentage of fines. Kondolf *et al*. (1993) showed a reduction in the amount of fines present by 37% and noted that the more fines present originally, the greater the cleansing effect of cutting. However, Porter (1985) and Crisp & Carling (1989) amongst others do not show a significant reduction in fines. Crisp & Carling state that there was little loss of fines, the primary effect of the cutting was to loosen the coarse sediment, potentially increasing the permeability of the gravel and much fine material was displaced to the bottom of the redd. However because of differences in sampling method and the definition of fines between the studies it is difficult to draw firm conclusions as to the cleansing effect of the cutting action. One problem is that different studies define 'fines' differently. The greater number of studies define fines as size fractions less than 1mm (*e.g.* Porter, 1985 and unpublished data 1987; Everest *et al*. 1987) but other 'cut-off' values have been used such as 2mm or 0.83 mm (McNeil & Ahnell 1964; Helle 1970; and Ringler 1970).

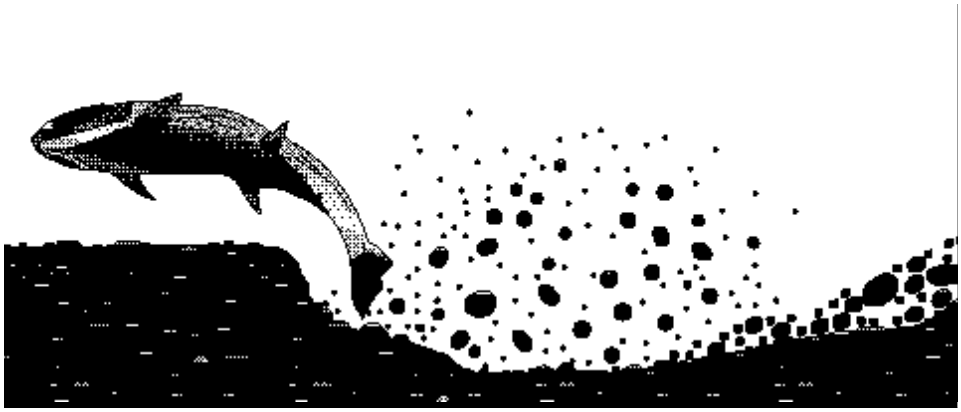

Figure 1.1 A salmon cutting a redd. From Alonso *et al*. (1996)

Theoretically, burying eggs in loose river gravel allows the eggs protection from predators and physical abrasion, whilst an intragravel water flow driven by the surface streamflow provides a regular supply of oxygen from upstream whereas metabolic waste products are moved downstream. One of the main problems is that siltation by clay, silt or sand within the gravel void spaces will reduce the flow of water too and from the egg pockets. Most observers have remarked that the preferred sites chosen for spawning are in areas of significant downwelling or upwelling in the flow - for example at the downstream end of a pool, as the water begins to flow across a riffle. Where possible fish seem to choose 'clean' gravel for spawning. Possibly this is an adaptive strategy because the restriction of the intragravel flow by fine sediment already in the pore space might cause anoxyia in the vicinity of the eggs and further, upon hatching, would hinder the emergence of the young fish or 'alevins' from the gravel into the streamwater. Finally, organic components of fine sediment may contribute to the BOD of the water further reducing the oxygen supply to the developing eggs or alevins. Recruitment of young fish may thus be compromised if the spawing gravel is polluted with excessive fine sediments either introduced to the gravel before spawning or washed into the pore space after the redd has been constructed.

1.1.2 Statement of research problem

It is widely believed that the hummocky morphology of the salmonid redd induces a downwelling of the stream current such that oxygenated water percolates into the redd gravels by a process called intragravel flow. This percolation may be induced by stream flow turning downwards into the pot, and/or by the favourable pressure gradient exerted between the upstream and downstream faces of the tailspill inducing flow through the tail of the redd. Using crude dye tracing techniques the basic flow pattern through the gravel has been demonstrated in the field (Hobbs, 1937; Burner, 1951; Stuart, 1953) and in the laboratory (Cooper, 1965; Harrison and Clayton, 1970; Thibodeaux and Boyle, 1987). Natural and anthropogenic factors may cause increased intrusion and accumulation of fine sediments in the spawning beds, reducing permeability and the supply of oxygenated water to the embryos, and hindering the flushing of metabolic waste products. Chapman (1988) provides a comprehensive review of the impacts of fines on salmonid embryos. Chapman's review demonstrates that the quality of the spawning environment is controlled by multiple factors that act simultaneously whereas most scientific studies have reduced complexity by concentrating on single-factor analysis. Nevertheless sufficient understanding of the problems now exists for a model to have been developed to predict the effect of sediment intrusion on the dissolved oxygen status within redds of the North American Chinook salmon (*Oncorhynchus tshawytscha*) and the Steelhead trout (*Oncorrhynchus mykiss*) (Alonso *et al*, 1996). This Sediment Intrusion and Dissolved Oxygen model (SIDO) may prove applicable to UK salmonid species. However a number of key questions remain:

- The detailed mechanism whereby turbulent river flow above the redd drives the intragravel flow patterns has not previously been demonstrated.
- Laboratory studies have been conducted in narrow hydraulic flumes (*e.g.* Thibodeaux and Boyle, 1987) whereby flow passes over and through an essentially two-dimensional (2-D) artificial redd. Thus the applicability of results stemming from 2-D flume tests to fully three-dimensional (3-D) redds in broad flows has not previously been assessed.
- The patterns of 3-D intragravel flow through redds needs detailing.
- The SIDO model needs evaluating and calibrating for UK application.

Four key goals were identified for this programme:

- Quantify the detail of 'longitudinal' turbulent stream flow conditions upstream of and above a salmonid redd. To achieve this an essentially two-dimensional (2-D) artificial redd was created in a narrow (300mm wide) flume and 2-D flow experiments carried out using an Acoustic Doppler Velocimeter (ADV) to measure series of velocity profiles along a downstream transect.
- Quantify the detail of 3-D turbulent flow conditions upstream of and above a salmonid redd. To achieve this an artificial 3-D redd was created in a broad flume (900mm wide) and 3-D flow experiments carried out using a dense ADV sampling array in conjunction with some flow visualisation experiments.
- Visualize and quantify where possible, the nature of intragravel flow and demonstrate how the exchange mechanism with the free stream-flow operates.

- Assess and modify where appropriate the computer model SIDO for use in the UK.

2 METHOD

2.1 Laboratory Experiments

Studies of turbulent flow above an artificial redd and the induced intragravel flow were conducted in a narrow flume (300mm wide) and in a broad flume (900mm wide). The latter was of sufficient width to accommodate a full size salmonid redd whilst in the narrow flume only the long-profile of the redd could be recreated.

2.1.1 Selecting redd characteristics

Forming the gravel bed

The size of gravel in redds is largely a function of the geology of the catchment and the velocity of the river. However the female salmonid often shows a tendency to select gravels of a given size for spawning. Kondolf (1988) showed some similarity in the grain size obtained from a study of like-sized salmon in the literature. Kondolf & Wolman (1993), using many data sets from the literature, showed a general weak trend for larger fish to cut redds in larger gravel. Despite the importance of grain size information to studies on spawning gravel, there is no consensus on how to collect samples, measure grain sizes and record the information. For example, the definition of the term "fines" has varied from material finer than 6.35 mm (Thurow & King 1990) to material finer than 0.83 mm (McNeil & Ahnell 1964, Ringler 1970). In this study we screened natural river gravel to exclude those fractions finer than 4mm and coarser then 16mm such that the mean grain size was 8mm (see Figure 2.5). This gravel was used to form a flat bed 300mm thick in the flume; this depth is representative of the range of depths at which UK salmonids bury their eggs (Crisp and Carling, 1989).

Forming the redd

Figure 2.1 shows a common 2-D representation of a redd immediately after construction. The elevation difference between pot and tail may be reduced in amplitude by later high flows filling in the pot with gravel and eroding the tailspill. However usually redd structure is resilient to low to medium flow events. Of primary importance, from the point of view of the model, are the grain size data as well as the shape and scale of the redd immediately after egg burial. This can be seen from the following suppositions:

- the larger and better sorted the sediment, the greater the degree of turbulence in the stream flow and the faster the interstitial flow through the redd;
- the shape of the redd affects the turbulent flow structure above the redd;
- the shape of the redd affects the bilateral exchange of stream flow/intragravel flow;
- the depth of the egg pocket in the redd effects the exposure of the eggs to intragravel flow pathways of differing speed.

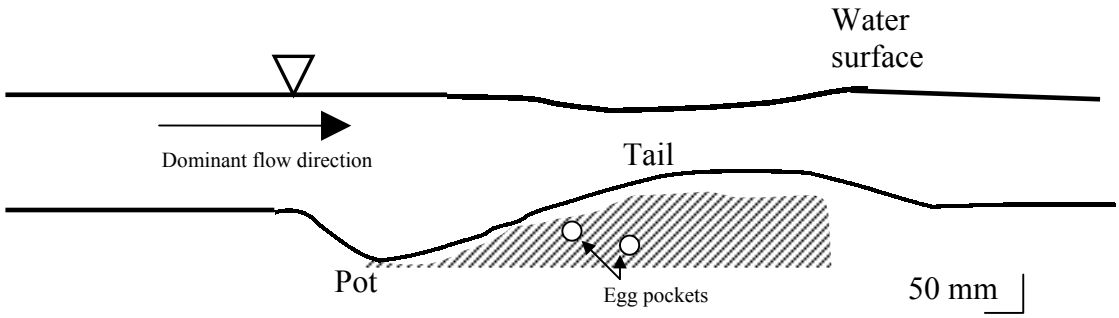

Figure 2.1 Transverse section of a 'typical' Brown Trout redd. Adapted from Ottoway et al. (1981). Shaded area is region where egg pockets are commonly encountered.

Figure 2.1 shows shows a longitudinal section of a Brown Trout redd. This form is representative of UK Brown Trout redds and also is typical in shape to Atlantic Salmon redds, although the latter are larger structures (Crisp and Carling, 1989). The scale of the redd can vary can depend on the behaviour of cutting female, the sediment gradation and the flow conditions. For example, the faster the flow, the more elongate the tail. Ottoway *et al*. (1981) and Crisp & Carling (1989) related the various dimensions of the redd to the speed of the current and size of the female cutting the gravel based on observations from UK rivers. The data sets used in both papers were limited to redds clearly associated with specific females. Ottaway *et al*. (1981) show a tendency for larger fish to spawn in deeper waters and for larger fish to bury their eggs deeper.

In an artificial laboratory redd the positioning of the egg pockets is of prime interest. Several studies have recorded the depth of the egg pockets (reviewed in DeVries, 1997). These studies show a wide range of values within species. In part this can be accounted for by the size of the individual doing the cutting in the same way that the other dimensions of the redd seem to be affected. Other relevant factors include the method of measurement - for example the choice of the datum level (*e.g.* the original bed level or the top of the redd tail). If a distinct egg pocket is found, the locus may be recorded as the top, centre or base of the pocket. The method of extraction used can also affect the reported measurements. Whilst freeze coring gives quite reliable data on the position of the eggs, manual excavation methods can disturb the position of the eggs giving erroneous results. Potentially, the eggs may have been subject to disturbance and reburial by scour (*i.e.* moved from their original position) or gravel may have been eroded or deposited above the egg pockets subsequent to redd excavation. Grost *et al*. (1991) demonstrated that in Brown Trout redds, the pockets are of increasing depth further downstream in the redd. Hence egg pockets are commonly encountered in the shaded portion of Figure 2.1.

The artificial redd was created by physically cutting it in a method similar to that used by the female salmonid. Rapid hand flapping (mimicking the female salmonid) caused lift forces to entrain particles into the flow. This procedure was continued until the dimensions of the redd approximated those of an actual redd (using data presented in Ottoway *et. al* (1981) as a guide). Cutting the redd in this manner means that when the gravel settles to form the tail, the orientation of the particles should be

similar to that of the particles in real redds. The shape of the redd formed is shown in Figure 2.2 (p.8). The pot measured approximately 400mm long and the tail an additional 600mm. The topography of the redd was recorded on a 20mm by 20mm grid by using a vertical point-gauge attached to a trolley running on rails above the gravel. The point-gauge is linked to a Vernier scale, allowing measurements with a 0.1mm precision. However, given the unstable nature of the individual particles at the bed surface, this was considered to be too precise, and instead measurements were recorded to the nearest millimetre. Templates of the shape of the bedform allowed checks to be made of bed stability and minor repairs to the redd geometry between tests.

2.1.2 Sampling the turbulent flow with ADV

Although redds are cut in gravel bed rivers, the actual environmental conditions such as flow speed and bed slope vary considerably between sites. The slope of the gravel bed surface was representative of gravel bed rivers (0·008 to 0.01). The depth and approach velocity (see RESULTS) were consistent with conditions pertaining to UK salmonids (Crisp and Carling, 1989), resulting in flow settings which included the highest possible before bed load transportation occurred.

Measurement and interpretation of turbulent flow data is a highly specialised discipline. Full details are contained within an M.Phil. thesis (Taylor, 2000). In brief turbulent flow moves not only downstream (*x*-direction) but also horizontally (*y*-direction) and vertically (*z*-direction) so it is possible to conceptualise of orthogonal *time-average* and *fluctuating* velocity series in time at any one point in the flow. Thus $U = \overline{U} + u'$, $V = \overline{V} + v'$ and $W = \overline{W} + w'$ where U is the streamwise flow component, and V and W are the vertical and horizontal components respectively. Overbars represent the time-averaged values and prime values represent fluctuating values about the mean values. The root mean square of the fluctuating component (in a long enough time series) can be used to give an indication of the amount of variation.

Using an acoustic doppler velocity meter (ADV) it is relatively simple to measure the three components of flow *simultaneously* and, by manipulating the data, the nature of turbulent eddies can be identified. Thus if the presence of the artificial salmonid redd in the test flume alters the flow, it is possible to measure and map the structure of the flow.

The ADV was securely fastened to a trolley running along rails on top of the flume. High frequency (25Hz) velocity measurements were obtained simultaneously in the three orthogonal directions. The sample volume was 50mm and as measurements taken close to the bed may be suspect, replicate measurements were taken close to the bed until consistent readings were obtained.

The sampling strategy used with the ADV is shown in Figure 2.2 (this is a longitudinal section through the test section of the flume). The top 50mm of the flow adjacent to the water surface cannot be measured using the ADV. It is worth noting that in these 2-D tests the water level is drawn down downstream of the crest of the bedform and never fully recovers to match the upstream depth. This is an artifact of the narrow flume but replicates the nature of flow recovery above some natural redds

in shallow water. In the 3-D tests draw down recovered rapidly downstream of the crest.

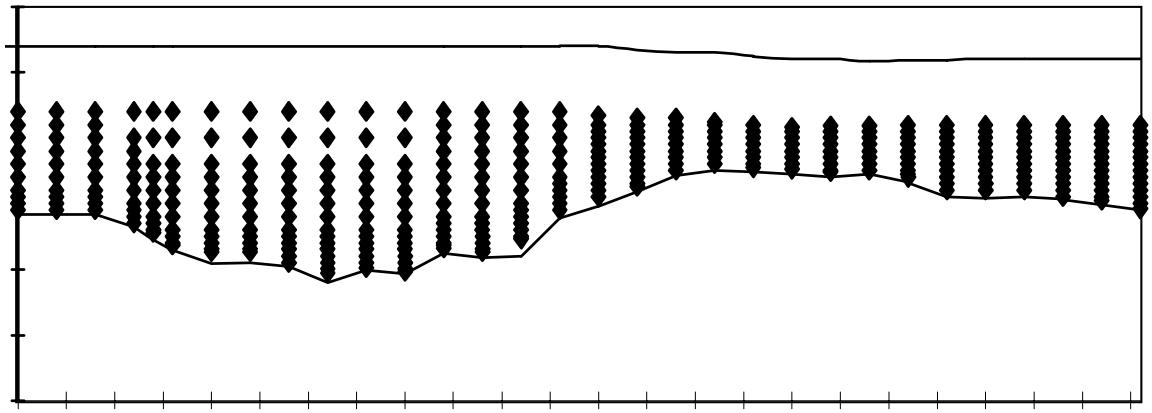

Figure 2.2 A long-section in the narrow flume: note the profile of the redd, the velocity sampling points and the draw-down in water level. (Flow left to right).

Slight variations in flow rate (known as hunting) occurred over the course of a test run. This is common in flumes and is a result of mechanical limitations with the pump. In order to create steady flow, the pump was always run for an hour before sampling started. At the start of each measurement session, the first set of points (a vertical profile) was recorded at a given position at the upstream end of the flume. This allowed some basic comparison of the entry flow properties of the flume during the subsequent replicate sampling sessions. In all areas (except near the top of the vertical profiles in the pot) the sampling points are separated vertically by either 5 or 10mm. Near bed sampling points were spaced at 5mm. Each point was sampled for at least 120s at the maximum sampling rate (25Hz) producing 3000 measurements of each orthogonal component. In areas which produced noisy data (generally, those near the bed), a longer sampling time between 180 and 300 seconds was used.

The sampling grid is pictured below in plan view (Figure 2.3). In the 2-D tests only the longitudinal profile was sampled. The cross-stream sections are positioned such that they align with the upstream end of the pot, the deepest part of the pot, the crossover region between the pot and the tail, the crest of the tail and approximately half way down the tail.

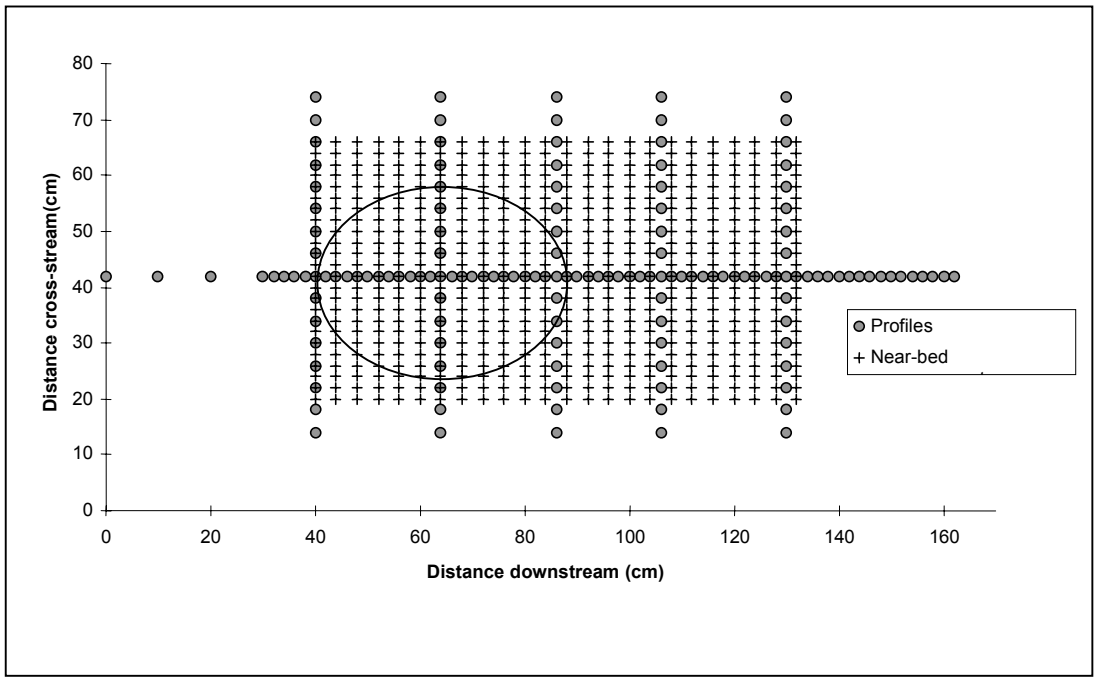

Figure 2.3 Plan view of the sampling grid used in the 3-D experiments. The marked oval corresponds to the approximate shape of the pot of the redd.

An extensive sampling strategy was required to get sufficient data to define the flow patterns around the redd. The high level of turbulent activity around the redd, meant that the maximum sampling rate was required. Thus it was necessary to compromise the need for an extensive sampling grid with the need for long sampling times. This meant that the time taken to both sample and analyse the results was large. Consequently the number of flow conditions that could be studied was restricted to one case for the 2-D tests and two cases for the 3-D test:

- The 2-D flow condition represented a very stable bed environment. The approach depth was 0.152m, the section-averaged approach velocity was 0.385m s^{-1}. The bed slope was 0.01 but the redd itself disturbed the water surface such that locally the water surface slope varied between 0.004 and 0.21.

- The two 3-D flow conditions represented a stable bed and a bed near initial motion. The approach water depths were 0.125m or 0.145m respectively. The velocity was 0.527m s^{-1} or 0.578m s^{-1}. The bed slope was 0.01 but the water surface slope varied locally between 0.007 and 0.01. The error bounds (60% confidence) were S=0.012±0.002 above the tail. However, repeatability of the water surface was very good and control was achieved by altering the flow rate that was monitored by an orifice plate (before the inlet tank) and an associated water level manometer.

The parameters calculated were the mean flow fields (U, V, W and $\boldsymbol{U}$, the total flow velocity), the root mean squares of the distributions, the skew values of the distributions, and turbulence intensity, Reynolds stress tensors and the proportion of quadrant 2 and 4 events (representing flow pulses moving away and towards the bed respectively: see Taylor, 2000 for full details). The mean flow velocities were the

mean values of the velocities measured in the sampling period (i.e. over the three thousand measurements per mean value). The calculation used for the root mean square velocity is shown in expression 2.1 and the skew values in expression 2.2. The Reynolds stress tensors are calculated using expression 2.3. The turbulence intensity is defined in expression 2.4. As such, this latter measure of flow highlights regions of high turbulence but low average flow.

$$u_{rms} = \left[\frac{1}{n} \sum_{i=1}^{n} (u_i - U)^2 \right]^{\frac{1}{2}} \quad [2.1]$$

$$u_{\text{Skew}} = \frac{1}{n} \sum_{i=1}^{n} \left[\frac{(u_i - U)}{u_{rms}} \right]^3 \quad [2.2]$$

$$\text{Re}_y = -\rho \frac{1}{n} \sum_{i=1}^{n} (u_i - U)(w_i - W) \quad [2.3]$$

$$\text{TI} = 100 \times \boldsymbol{u}_{\text{rms}} / \boldsymbol{U} \quad [2.4]$$

The parameters extracted from the data sets were then re-arranged and plotted using the software "Spyglass" in both two- and three-dimensional formats. This allowed ready visualisation and easier identification of the flow characteristics (especially with respect to their relation to the redd geometry).

2.1.3 Intragravel flow visualisation

Dye visualisation

Taylor (2000) considers the use of a variety of intragravel flow monitoring techniques based on KCl solution or using spheres of benzoic acid as tracers. These methods were rejected for a variety of practical reasons. Preliminary intragravel flow visualization experiments in the 2-D representation used a peristaltic pump to inject dye (Methylene Blue) via tube into the gravel bed adjacent to the glass flume side-wall. A video camera recorded the results. Pumping liquid into the pore spaces during the flow will disrupt the natural flow patterns to be recorded. Hence, the pump was set to a low flow rate (the dye had to be used in concentrated form to compensate) to reduce this problem. The tubing was inserted vertically into the existing gravel bed at several points along the 2-D redd long-profile. In the 3-D representation one half of the model redd was rebuilt with its central plane at the glass side of the flume to check that flow paths below the bed were in agreement with Cooper (1965), and to contrast these with the case of a plain bed. These tests used Methylene Blue as a visual tracer.

Passive dye detection

Granular activated charcoal was used to make passive dye detectors, which were analysed after each experiment. It is argued here that the adsorption of dye from the intragravel flow by the charcoal reflects the process of dissolved oxygen removal by developing salmonid eggs and is therefore an especially suitable technique. Dissolved oxygen is not easy to control in a flume and there were insufficient equipment available to measure it in 3-D arrays within the redd. Instead Rhodamine WT was used as tracer, representing dissolved oxygen; and granular activated charcoal was

used for tracer detectors, representing the eggs. This technique was justified for three reasons:

- Several locations could be sampled, either above or below the bed, without disturbance of the gravel in the artificial redd during the experimental run, unlike techniques involving sampling tubes, or larger instruments which disturb the environment.
- The interaction of salmonid eggs and dissolved oxygen is a diffusion process from across a laminar flow layer adjacent to the boundary (i.e. the egg's wall). The same physical process governs dye accumulation in the activated charcoal detectors placed in the flume, at least as long as active sites in the charcoal remain available. Though the detector results give only relative values, we ought to expect them to be relevant to egg survival since the physical exchange process is the same. Clearly, the egg's oxygen consumption process is not modeled by the flume experiment.

- The technique should be applicable in experiments in the laboratory or field where the influence of added fine sediment to the intragravel environment is considered.

Detectors were made by taking M8 zinc-coated steel nuts, and dipping one end face only into clear varnish and then into the granular activated charcoal. The detector was then placed charcoal-side down on a plastic sheet and left overnight to dry. This could be done with reasonable consistency after a little practice. The detectors were always placed charcoal-side down in the flume, and their vertical position was recorded by a tape measurement to the gravel top surface.

After several initial trials, the dye extraction technique was standardized using solvents. The dye solutions in test tubes were then placed in the fluorometer and a reading of Rhodamine concentration in parts per billion taken.

Two quantitative dye tracing experiments were done on the 3-D artificial redd in the 900mm wide flume. The dye quantities and run durations etc. were determined after two preliminary runs.

The 'plug' injection method: After placing dye detectors in the surface layer of the bed the required flow was established. The detectors were in groups of four, each group at about the same x-location, and within a 10mm wide strip along the centreline of the flume. To place the detectors the surface (armour) layer above the desired location was removed and kept in a separate container, and the gravel matrix below dug carefully by hand and placed in another container, minimizing disturbance of neighboring areas. Detectors were placed as the excavated hole was refilled. The surface layer was replaced and the surface detector group put in place. The size and shape of the redd was checked visually and with templates. Rhodomine dye (150mg), diluted in 1.5 litres of water, was then added to the flow as a 'plug' at the extreme upstream end of the flume. Attention was paid to achieving good uniformity of the plume in the transverse (y) direction. Vertical mixing was assumed, since the distance from the injection point to the first detectors was over 20 flow depths. The entire dye plume traveled down the flume in about 30 seconds and the flow was stopped before the plume returned through the sump to the upstream end of the flume. The detectors were then removed for analysis after leaving the bed to drain overnight.

The uniform concentration method: The dye left in the flume after the above run was diluted and thoroughly mixed by running the flume to obtain a uniform concentration of 3.75±0.05 ppb. The flume was turned off and allowed to drain. Dye detectors were then placed, in groups of four, at various locations, both below the bed and in the surface. These groups were again kept within the central 100mm of the flume. Flow was established as quickly as possible, without significantly disturbing the bed, and maintained for 20 minutes. The lowest placed detectors remained in the water for no more than 2 minutes longer than the highest. The bed was left to drain overnight, and the detectors were removed and analyzed the next day, each having its *z*-ordinate recorded.

During the uniform concentration run some extra detectors were placed on wires, both on the bed and below it, so they could be removed at (roughly) exponential time intervals. These provided a test of linearity for the technique. At the end of the uniform concentration run some fresh detectors were placed in a container surrounded by bed material gravel, which was then placed in the still water in the flume inlet tank for the same duration as the experiment had run for (20 minutes). The dye extractions from these detectors provides a result for zero intragravel flow rate under the same duration and concentration conditions as found in the experiment. All experiments had a group of detectors placed in the free-stream flow, about 50mm above the bed.

2.2 SIDO-UK Model

2.2.1 Introduction

The computer software SIDO (Alonso *et al.* 1996) was developed for application in North America and was calibrated for Chinook Salmon and Steelhead Trout in the Tucannon River. In this report the model was first converted from imperial to metric units and the computational grid within the redd was made finer. Using results from the flume studies improved information is available on the near-bed flow boundary conditions, such that the modelled interstitial flow can be checked against the flume flow data. In the same way that cells can be defined based on the filling status, the flow-through cells can be defined on whether the flow through them is Darcian or turbulent. However the main methodological reconfiguration consisted of reparameterizing the code using data pertinent to UK salmonids obtained from the literature. Species-specific and habitat-specific conditions and parameters have been changed in order to more accurately represent the UK situation (see Appendix). Whilst the SIDO model has been used on large scale rivers in the USA, in its application to a UK upland gravel bedded river, the major differences will result from the flashiness of the hydrograph response and the resulting supply of suspended sediments. Throughout this report the revised code is called SIDO-UK.

2.2.2 Location and overview of available data

A typical UK upland gravel bed reach on the River Lune was selected, for which much of the required data was available, or could be inferred from other measurements on similar regimes in the North of England. The reach selected was a straight section with a relatively large bed slope synonymous with typical spawning locations, and typical cross-sectional topographical detail from Page (1998) are given

in Figure 2.4. Characteristic bed material size information was obtained from a study just upstream of these cross sections, from the MPhil thesis of Orr (1996). A hypothetical daily mean hydrograph had to be constructed from a record of daily high discharges (Environment Agency) that was available for a gauging station just downstream of the site, although unfortunately a tributary joined the Lune between the site and the gauging station. Monthly temperature information (Crisp, 1990) was also available for the Lune at Denny Bridge, although this is considerably further downstream. Measurements of egg burial depth and redd pit and tail length dimensions that were made by Crisp and Carling (1989) for Atlantic Salmon and Brown Trout in rivers in the NE of England. Measurements of the finer fractions bed material composition that were taken from redds come from the same study. Rating relationships for suspended sediment load come from a study by Carling (1984) of Great Eggleshope Beck, which is located in the North Pennines.

2.2.3 Species dependent information

There are a number of biological factors which vary between the species, such as number of eggs laid (Elliot and Hurley, 1998). These differences have been included in the adjustment of SIDO for UK use in Table 7.1. Where information is available for Atlantic Salmon and Brown Trout, this is incorporated into the model. However, if the literature survey only produced information regarding one of these species, this was used for both salmonids, in preference to the American species data.

2.2.4 The principal physical parameters

SIDO can be used to represent a changing hydrograph using a series of 1 day events, estimating antecedent stream flow conditions above the bed on the basis of mass conservation and energy head loss considerations. Surveyed cross-section details for a relatively straight section of reach with a relatively steep gradient (0.0064) are shown in Figure 2.4, after Page (1998). The hypothetical hydrograph (see Fig. 2.5) used was assumed to be typical of the daily discharges for the upper Lune over the spawning season from October-March. Because of the tributary (of approximately equal size to the Lune) between the test site and the gauging station at Lune's Bridge, the recorded daily high flows were divided by a factor of 2 to produce flow magnitudes and a flood frequency that were not unrealistic for the site. The hydrograph was therefore only representative of the local response of the Lune, but it is known to be exceptionally flashy, and goes over bank several times a year with discharges between 23-40 m^3s^{-1} (Orr, 1996). Although a record of daily mean flows at Lune's Bridge was not obtained during the course of this research, the use of the daily high flows record in SIDO ensures that the important events when most sediment transport occurs are not overlooked.

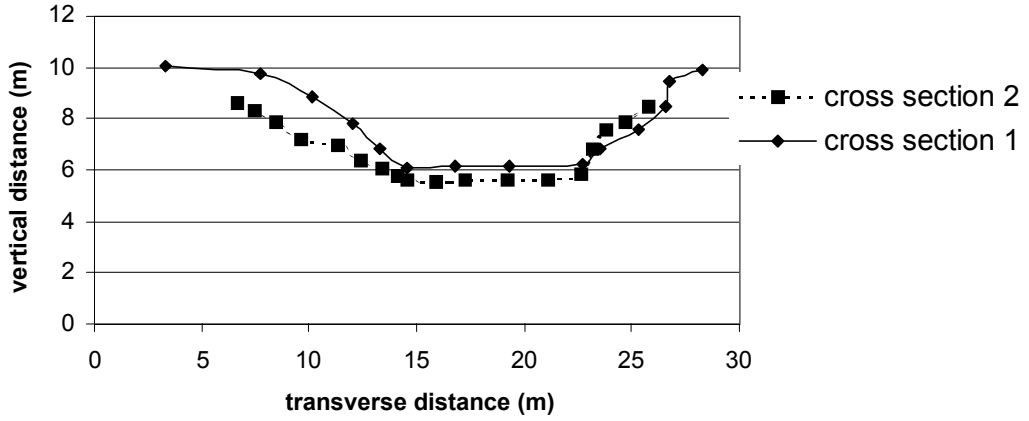

Figure 2.4 Example of cross-sections from engineered part of upper River Lune

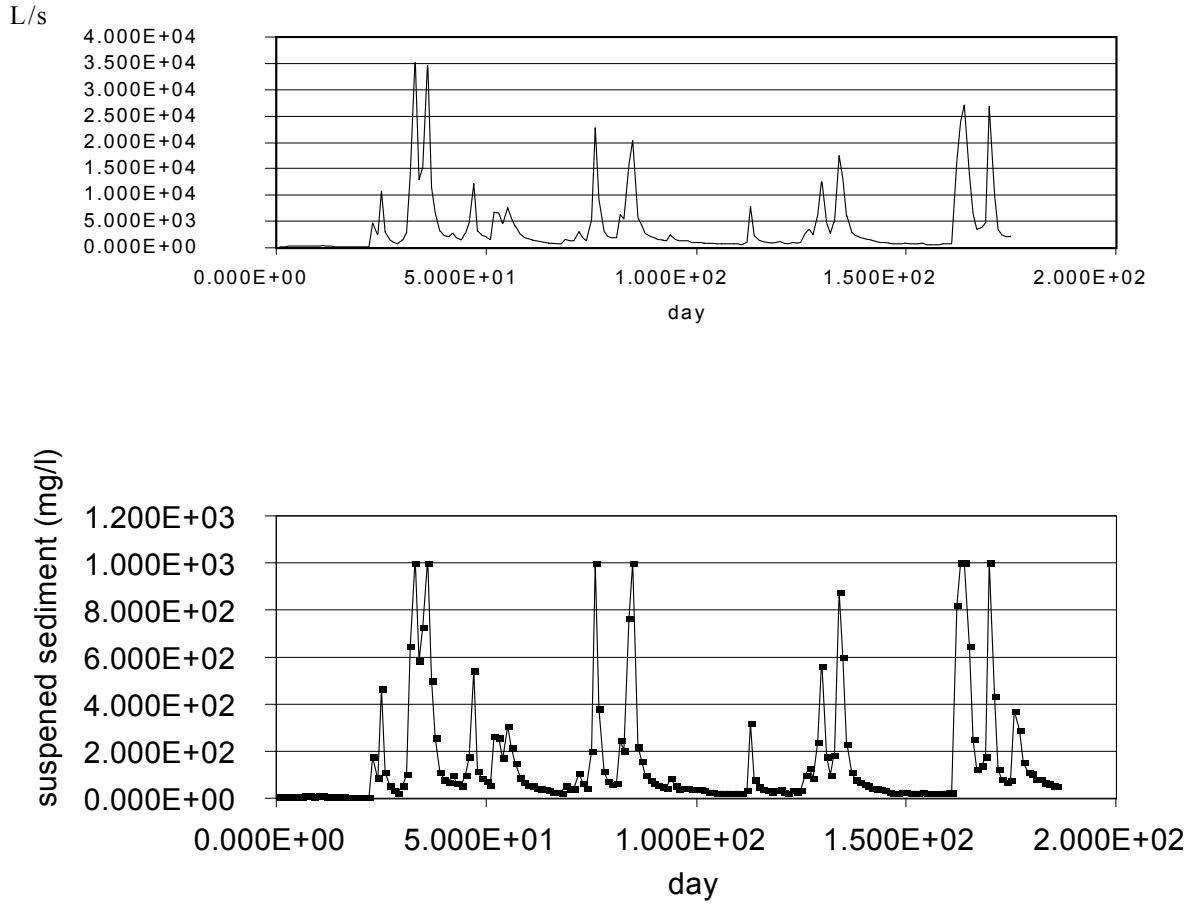

Figure 2.5 Example of hydrograph (above) derived from Lunes Bridge data (Sept-March 1995) and (below) suspended sediment load resulting from hydrograph (after Carling, 1984) with maximum threshold 1000mg l^{-1}

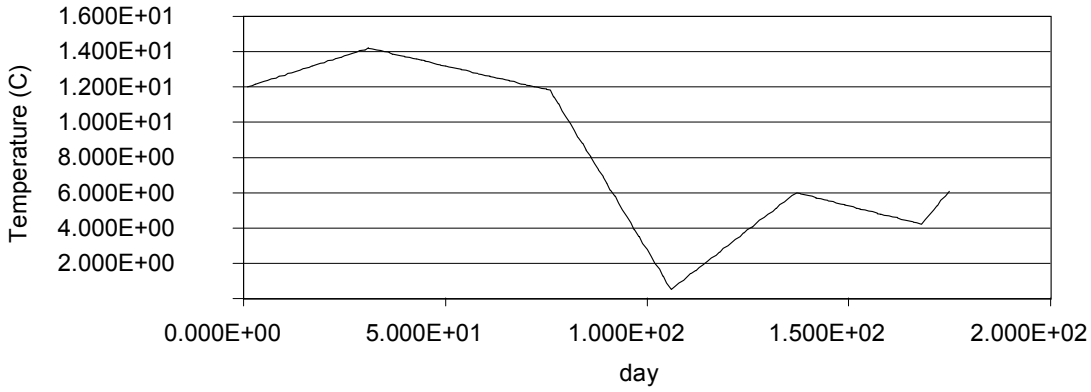

Figure 2.6 Linear interpolation of monthly mean water temperature in Lune at Denny Bridge (Sept-March 1995)

2.2.5 Suspended sediment loading

Additional information, regarding the discharge dependent concentrations of suspended sediments (SS) and estimations of Manning's roughness coefficient for the reach are also necessary. A relationship between suspended sediment load and discharge for a northern upland stream with a similar bankfull discharge to the river Lune at the test site was obtained from Carling (1984) for discharges up to 10 m^3s^{-1} in Great Eggleshope Beck (GEB). The relationship is a quadratic, and was determined from measurements in flows up to bank-full. However, it predicts the SS load at the depth at which samples were taken, whereas the suspended sediment close to the bed is required for accurate estimation of sediment intrusion.

In Carling (1984) the measurements of SS load were made at 10cm height above the bed using a pump, and at mid depth with a bulk sampling technique. Here the mid depth values are used, and then corrected using the Rouse equation (equation 3) to estimate the SS concentration near to the bed (Simons and Senturk, 1977), making the assumption (after Carling, 1984) that for this rough bedded river, the sediment distribution is fairly uniform throughout the depth.

$$C/C_a = \left((d-y)/y * \left(a/(d-a)\right)\right)^{Z_l} \text{ (equation 3)}$$

C = suspended sediment concentration at height = 0.01d (i.e. 1cm above bed for 1 meter flow depth). Ca is the concentration of suspended sediment with a certain fall velocity at a level y=a×d above the bed. d is the flow depth. Here Ca is known at a=0.5 of the depth. Z_l is estimated as 1/32 using the value from Simons and Senturk (1977) for a well-mixed flow. More accurate values of Z_l can be estimated from fits to measurements of SS at more than one point in the vertical. Carling and McCahon (1985) also found very little depthwise variation in SS concentrations, supporting the use of a small value of Z_l . Having determined the relationship between the SS close to the bed and that at which the measurements were made, a modified SS rating curve was produced, which was then used to produce Figure 2.5 (lower).

Because the hydrograph includes spates of greater than bankfull flooding, it was assumed that for over-bank flow there was no additional sediments made available per unit width of flow. A maximum threshold of 1000 mg/l was imposed on the suspended sediment record for the Lune test site, compatible with the maximum observed bulk sample from GEB, which was 818mg/l (mostly silt) from Carling (1984). For this reason SIDO input file **Hydrolog.inp** only has a *silt fraction* for scenarios A and B. This could be a crucial factor, as the impact of fine sediment on salmonid redds may be dependent on the size of the deposited sediment (Acornley and Sear, 1999).

Fine sands and silts tend to fill the intragravel pore space from the bottom up, resulting in a reduction in redd permeability, and therefore oxygen supply. Coarser sediments may result in a seal, although SIDO does not model this effect, it may inhibit alevin emergence.

2.2.6 Redd material composition and rate of infiltration of fines

The infiltration of fines into the intragravel substrate is believed to be one of the most critical conditions affecting the depletion of oxygen flow to the buried eggs. Since the pore space and redd material construction are controlling factors to this intrusive process, it is necessary to estimate conditions that are typical to UK rather than US rivers. Information regarding the finer materials found in the redds (<1mm) studied by Crisp and Carling (1982) was used to define the finer fractions in the different parts of the modelled redd. Here it was assumed that the undisturbed, disturbed and egg burial zones of Alonso et al. (1996) correspond roughly to the redd surface zone measurements of Crisp and Carling (1989). The larger sediment fractions were estimated from direct measurements of D_{50} at the upper Lune site by Orr (1996), and the intermediate fractions were linearly interpolated between the two. It should be noted that SIDO does not account for fines infiltrating from bedload storage.

2.2.7 Salmonid redd characteristics

Originally this study was to investigate redds with dimensions characteristic of Brown Trout and Atlantic Salmon. However, salmon redd dimensions such as redd tail length and pot length are highly dependent on fish size (Crisp and Carling (1989)), and since spawning salmonids have a large range of sizes (Crisp, per. comm.), it would appear more useful to future studies to use redd dimensions in the model which correspond to different ranges of salmonid size, as oppose to using redd dimensions corresponding to just two species (the SIDO model is set up to hold information for two species). Using data from Crisp and Carling (1989), redd dimensions were set up to correspond to the mean fish size (45.5cm), covering different species found in the NE of England (from a sample of 21 salmonid females).

Using regression equations relating fish length to pot and tail length respectively (Crisp and Carling, 1989) values of pot and tail lengths were determined as 81cm and 142cm respectively. The horizontal distance between trough and peak of the redd can be estimated from the average of these two characteristic lengths, to give: L=(81+142)/2=111cm, where L is the redd half wavelength. Further, using data from the same paper for a fish of 45.5cm length the amplitude (D) of the redd was

determined: D = 14.2cm. An estimate of the entry and exit angle (BETA in Alonso *et al.*, 1996) into the pot is required for the model and is given by : BETA ≈ atan (2D/L)

$$BETA_{b.trout}=atan(28.4/111) =14.3º.$$

This compares with the angle of 14º used for Steelhead Trout in the USA.

Elliot (1984) found less correlation between female size and egg burial depth, or redd length. From this latter study in Black Brows Beck, for a 45 cm fish, it was found that the typical redd depth and length were D=17cm and L=130cm, giving BETA=27.6º.

2.2.8 Salmonid biological characteristics

The suite of species dependent parameters relating to the oxygen consumption at the different stages of egg development include diffusivity coefficients to represent the rates of transfer of oxygen through the egg walls, the dimensions of which must also be characterised. This has been obtained from numerous references, but the most important being Carling (1985) and through personal communication with both Prof. Malcolm Elliot at the Institute of Freshwater Ecology, and Dr. Trevor Crisp.

The length of period between egg deposition and alevin emergence has been estimated to be between 84 and 100 days (Acornley, 1999). Acornley also found it takes approximately 25 days for levels of fines in redd to increase to concentrations found in undisturbed gravel.

Hamor and Garside (1976) found that oxygen concentration (of primary importance), rates of water exchange (secondary importance), and temperature (tertiary importance) considerably influenced survival of Atlantic Salmon embryos.

2.2.9 Temperature and salmonid egg development.

Water temperature affects the solubility of oxygen, and also directly affects the rate of development of salmonid eggs (Crisp,1981;1988; Acornley, 1999). However, Crisp (1990) suggests that in an upland stream, although eggs incubated within the gravel bed hatch earlier than those incubated at the gravel surface, the timing of alevin emergence varies little, regardless of egg burial depth. Elliot (1984) quotes degree days before hatching for Brown Trout: 50% eggs hatched and 50% alevins emerged after 444 degree-days and 852 degree-days from fertilised eggs in both the laboratory and a stream. Elliot also cites 0-25 degrees as the critical range of temperatures between which Brown Trout eggs can survive. Humpesch (1985) found that there was a minimum hatching temperature of 1.0ºC, and an upper in the range 10-16ºC, with an optimal temperature of 5ºC for Brown Trout.

2.3 Dissolved Oxygen and Salmonid Development.

The critical survival range of oxygen concentrations was estimated as falling between 0.00013-0.0003 mg egg^{-1} hr^{-1} for Atlantic Salmon by Wickett (1954), with a lethal oxygen level for hatching Chum Salmon of 2ppm at 5^{o} C.

2.3.1 Flow rate in gravel and salmonid development

The flow rate through the gravel substrate is also critical for egg survival, and is largely controlled by the parameter CPERM in SIDO. CPERM is recommended to be varied between 0 and 100, such that it generates an average intragravel flow rate that allows for the complete flushing of the redd in 1day. The value of 0.92 for CPERM, which was used for the US example gave an average interstitial velocity of 0.0192 cm s^{-1} for the application to the River Lune (Scenario A). For the 6m long redd domain, the time for complete flushing is therefore 600/0.0192 s, which is 8.7 hours. Therefore this value of CPERM was retained.

2.3.2 Days to hatching algorithm

The SIDO model takes the parameters of temperature and local dissolved oxygen level calculated each day, and uses the algorithms (in the sub-program EOC.f) given below to estimate hatching time:

$$H_t^{steelhead} = 10{,}747[(T+6.0)^{-2.0961}][1-0.88T(D_o - D_{os})]$$
$$H_t^{chinook} = 8253[(T+6.0)^{-1.8126}][1-0.88T(D_o - D_{os})] \quad \text{(equations 1a-1b)}$$

where T is temperature, D_o is the dissolved oxygen concentration, and D_{os} is the saturated dissolved oxygen concentration for the given temperature.

For UK species, the only compatible empirical relationship that was found in the literature also relates hatching time for Atlantic salmon to the dissolved oxygen level, the temperature *and the flow rate* (Hamor and Garside, 1976):

$$\log_{10} H_t^{At.Salmon} = 3.12 - \log_{10} 1.33T - \log_{10} D_o - \log_{10} 0.67F \quad \text{(equation 2)}$$

where the additional parameter is F, the flow rate (ml/s). This relationship can be found in module TOD.for of the SIDO code. It was found that these relationships gave comparable results for cases where the oxygen levels were reasonable, but that when the redd silted up and there was a rapid reduction in flow rate, equation 2 predicted a rapid increase in expected hatching time, as one might expect. The original hatching times predicted by SIDO remained relatively unchanged (see Table 2.1), since the D_o level and temperature can remain relatively unaffected by the redd filling up. Table 2.1 was compiled from run time output of SIDO. Clearly the predicted hatching time for Atlantic salmon is more realistic.

Table 2.1 Predicted hatching times results for scenario B, as predicted using equation 1a above (for steelhead trout) and equation 2 (for Atlantic salmon)

T	D_o	F	$H_t^{steelhead}$ (Equation 1b)	$H_t^{At\ Salmon}$ (Equation 2)
12.00	0.0107	0.0163	25.15	9.85
12.15	0.0045	0.0164	26.35	23.07
14.15	0.0035	0.0163	21.51	25.49
14.09	0.0036	0.0027	21.64	151.5

2.3.3 Fry emergence algorithm

SIDO determines the percentage fry emergence from the empirical relationship of Theurer and Miller (1986) between observed fry emergence and sediment mass percent finer than 0.85mm (PF085) and mass percent finer than 9.50 mm (PF950) for the entire disturbed portion of the redd domain:

Chinook Salmon PERFRY = 93.4 - (0.171 * PF950 * PF085)+(3.87 * PF085)
Steelhead Trout PERFRY = 94.7 - (0.116 * PF950 * PF085)+(0.007 * PF950 * PF085), where negative values are set to zero, and those in excess of 100 to100. It is considered that this is a particularly weak part of the SIDO algorithm (see sub-program Emerge.f), as there are a host of other known factors, in addition to the sediment filling that can affect fry emergence (Elliot, pers. comm). Consequently emergence predictions should be acknowledged to have large uncertainties. A similar algorithm for UK species was not found in the current literature survey.

3 RESULTS

3.1 Three-Dimensional Turbulent Flow around Redd

For the sake of brevity only the longitudinal data for one set of 3-D data are reported here. Detail of the transverse data are reported fully in Taylor (2000). Pertinent remarks concerning the 2-D results are referred to in the DISCUSSION. The flow characteristics measured for both 3-D tests runs are recorded in table 3.1. The main points sampled are shown in figure 3.1 below. The topography is detailed in Fig. 3.2.

Table 3.1 Summary table of flow properties. Multiple values refer to point *a* upstream of the pot, within the pot (around point *b*), above the tail (around point *d*) and downstream of the redd (along the plane of symmetry). (i) refers to first test and (ii) to second test.

Flow Property	**Value**
Water Temperature (ºC)	17-30
Flume Slope	0.0085
Water Depth (cm)	(i) 14.5, 22, 8.5, 14 (ii) 12.5, 20, 6.5, 12
U (cms^{-1})	(i) 52.66, 35.61, 55.29, 36.95 (ii) 57.84, 36.35, 60.91, 37.47
Shear Velocity (cms^{-1})	(i) 9.56, 9.61, 8.03, 9.44 (ii) 9.03, 9.18, 7.42, 8.74
Froude Number	(i) 0.61, 0.42, 0.64, 0.43 (ii) 0.67, 0.42, 0.71, 0.44
Water Slope	(i) 0.01 (ii) 0.007

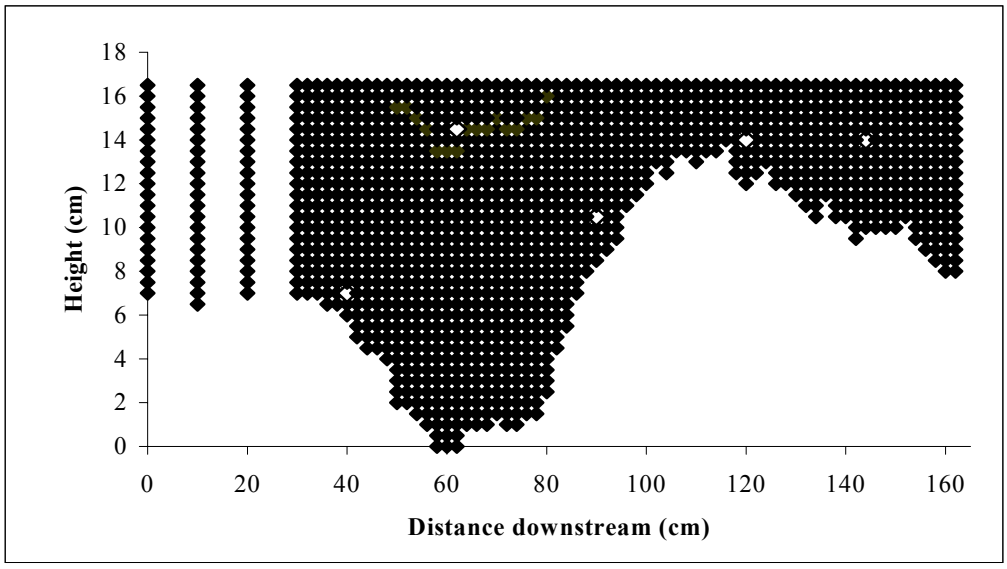

Figure 3.1 Sampling grid of the points sampled in the three dimensional case; along the central plane. The highlighted points are the points used for comparison in text.

a

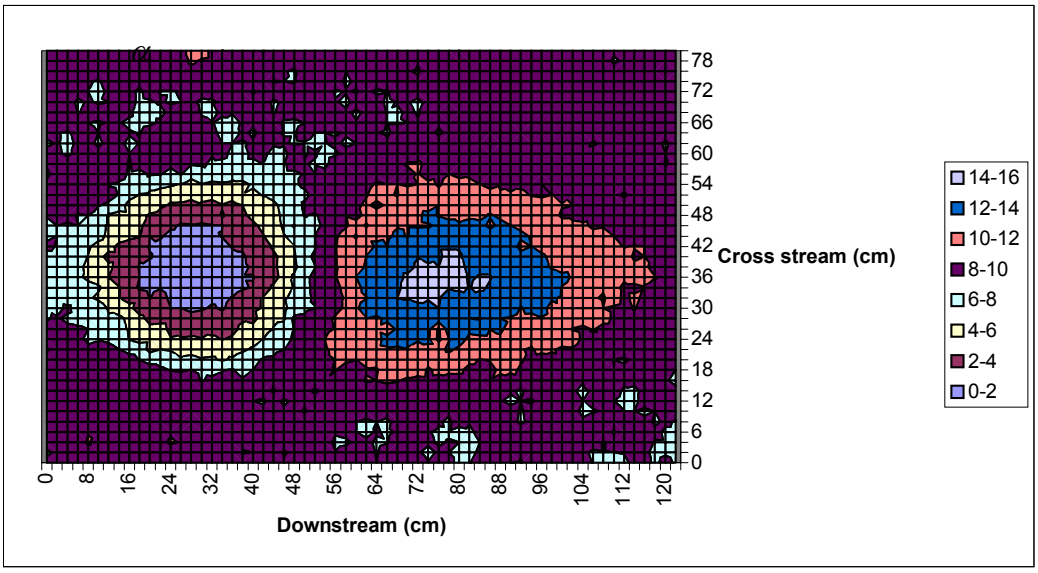

b

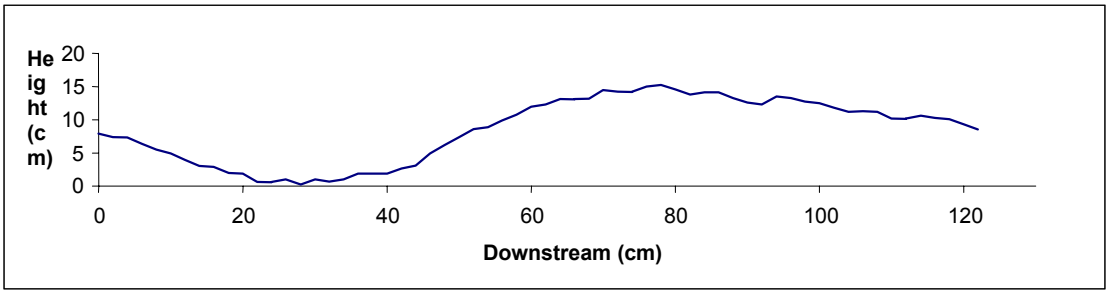

Figure 3.2 The topography of the three dimensional redd: a) plan view (scale in cm); and b) in section through the central plane. The angles α, β and δ have the values of 23.6º, 21.8º and 8.0º respectively.

3.1.1. Mean flow field

Figure 3.3, below, shows the mean flow field along the central plane in both the *x* and *z* directions (and the vector plot of the flow). It should be noted that the co-ordinate system used is a standard right-handed set with *x* directed downstream and *z* vertically upwards.

The mean flow field slows above the pot owing to flow expansion into the pot and to blocking of the flow by the tail of the redd. The flow then accelerates over the crest of the tail before slowing again downstream of the crest. Although not clear in Figure 3.3c (resolution problem), the region at the upstream end of the pot does show an area of reversed flow. This coincides with a relatively steep angle in the drop of the bed surface. It also occupies a region which has an upstream directed interstitial flow that was clear in the 2-D case. The flow in this area also has a positive *z* component, indicating that this is a complete re-circulation cell that might be better defined by other measures of turbulence considered later in this report. However the main flow cell in the pot occurs at the downstream end of the pot with water moving both downstream and strongly upwards over the upstream portion of the tail.

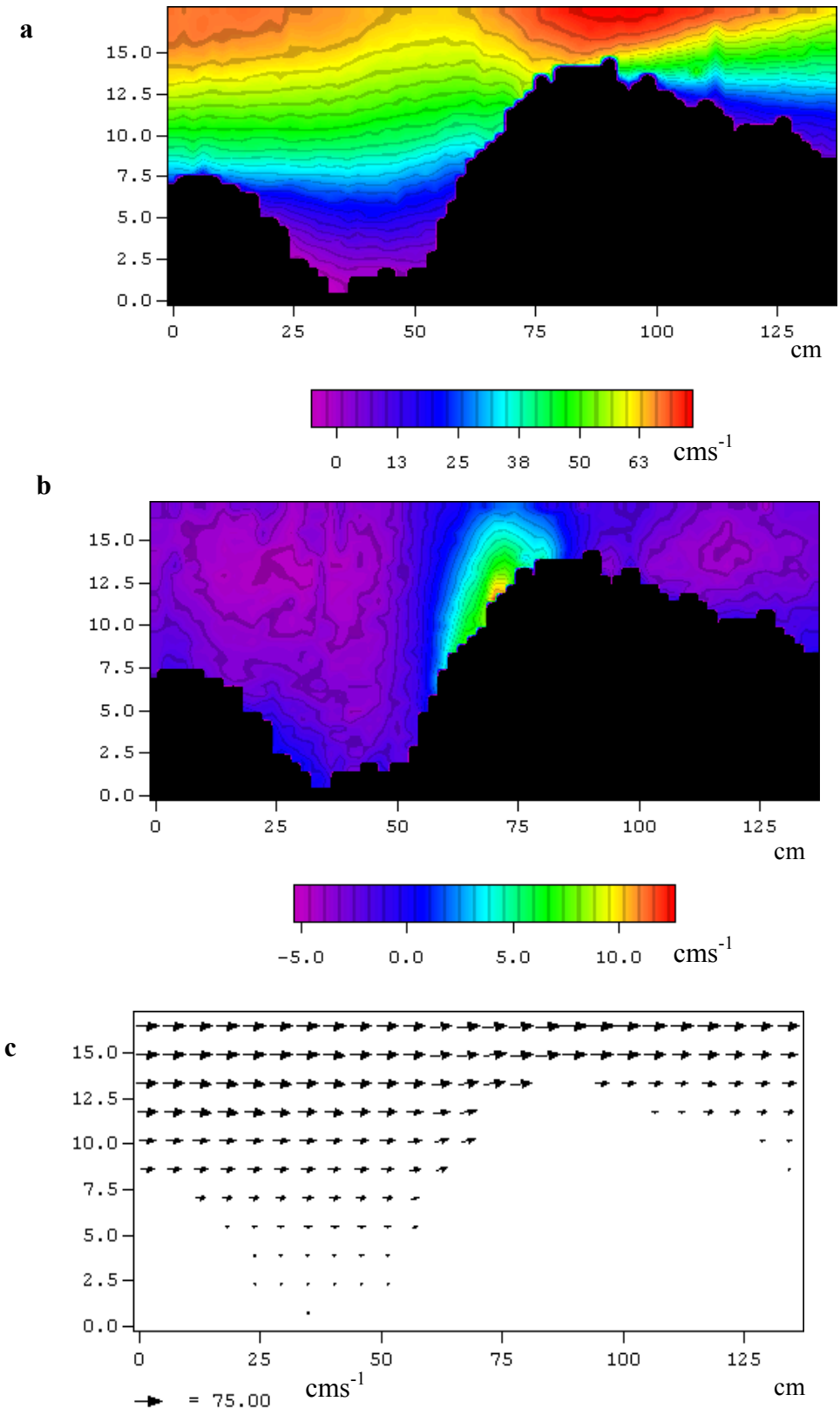

Figure 3.3 Mean flow field along the central plane. Shows a) Mean downstream velocity; b) Mean vertical velocity; and c) vector plot of the mean flow. The *x* co-ordinates used here are the defining set.

In comparison with the 2-D data, it should be noted that although the 2-D and 3-D downstream velocity components were similar in magnitude, the range was slightly greater in the 3-D case. Similarly, the 3-D case demonstrated a vertical velocity range twice that of the 2-D case. There are also some significant differences in the flow field as defined by selected streamlines. For example, selecting the 55cm s^{-1}streamline, the fastest flow region (red-orange) descends from the surface at a much steeper angle in the 2-D case (14º as opposed to 11º). The zone rises again at a different angle (3.6º in the 2-D case and 4.6º in the 3-D case). This suggests that the adjustment of the flow to the imposed topography of the bedform is quicker in the three dimensional case.

The significant difference between the 2-D and 3-D case is that in the 2-D test, the region of strongly upward flow extended to the crest of the redd where peak vertical velocities were recorded. This is evidently not the case in the 3-D representation (Figure 3.3). It was expected that the topographic forcing of the flow in the vertical would be more pronounced in the 2-D case as the bed was horizontal in transverse section and the flow was greatly constricted by the walls of the flume. The 3-D results show that although this forcing is somewhat relaxed when flow can diverge around the bedform, topographic forcing remains important.

Cross sections of the 3-D flow (not shown in this report) clearly show zones of flow divergence and convergence. The first cross section (x = 14 cm) at the upstream end of the redd shows flow down into the pot, both from above and from the sides. The second section (x = 38 cm) crosses through the deepest point of the pot, here the flow is downwards for the most part.

Cross section 3 (y = 60 cm), lies between the pot and the tail. This cross section shows the greatest variation in velocity. The flow field is picked out strongly in the vector diagram that shows a strong flow separation along the central plane of the redd as flow diverges around the tail. The vertical velocity in this cross section is not particularly high in comparison to the velocities in the positive and negative y directions. Section 4 (y = 80 cm, above the crest of the tail) shows a similar pattern, with the flow still responding to the topography although to a lesser extent. Finally section 5 (y = 104 cm – approximately half way down the tail), shows the flow finally converging back behind the crest.

3.1.2 Velocity moments and Reynolds stresses

Figure 3.4 shows the distribution of the root mean square (rms) values of the velocity distributions. The values for the root mean square velocities (in both the downstream and vertical direction) are of a comparable scale to the values obtained in the 2-D case.

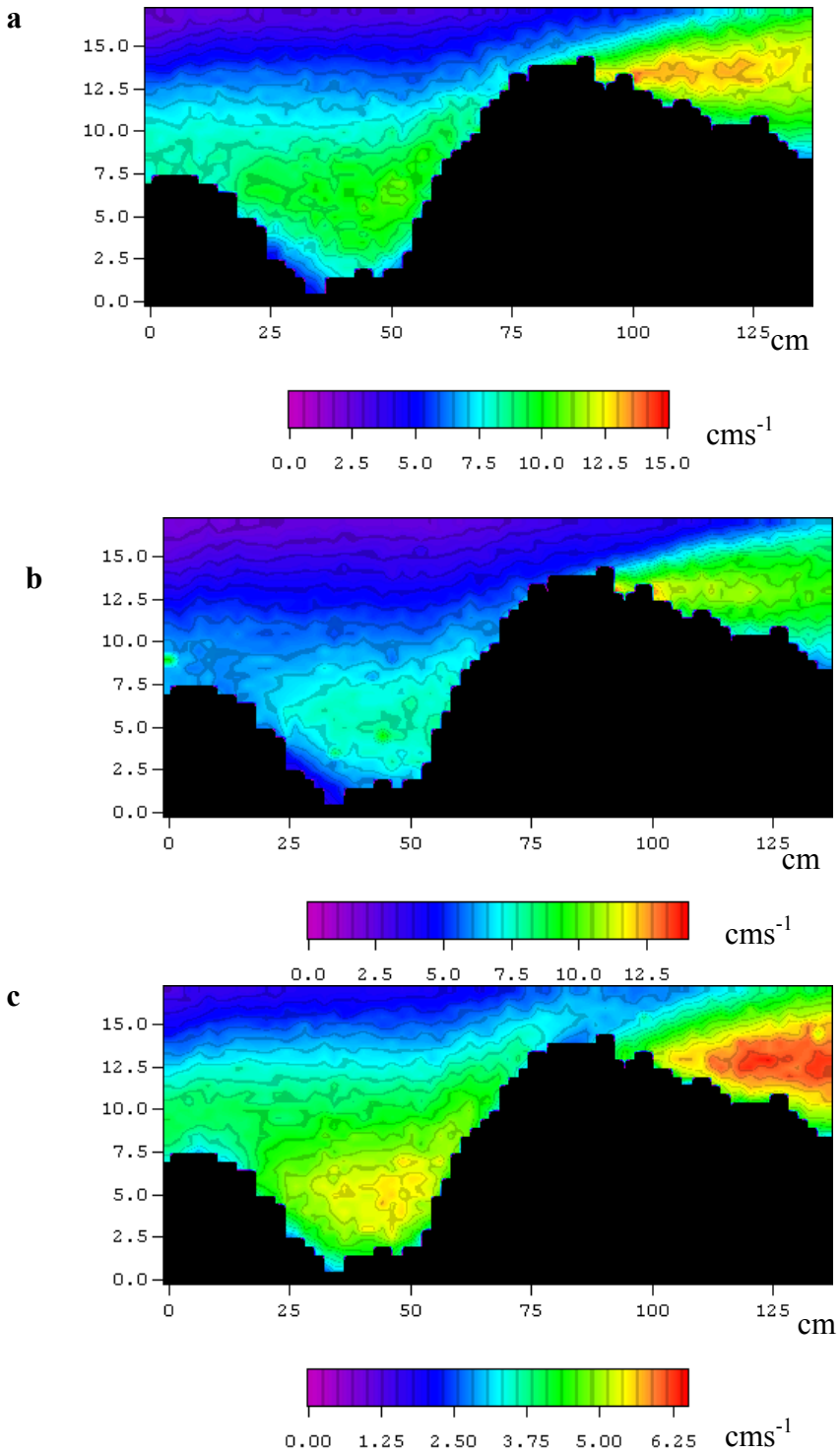

Figure 3.4 Distribution of the root mean square values of the velocities recorded in the a) downstream; b) cross stream and c) vertical directions.

The zones picked out by the 3-D data sets were clearly identified in the 2-D data as well. The angle at which the turbulent region downstream of the crest rises is slightly steeper (approximately 4-4.5º for the 3-D case). The 3-D data show greater detail of the character of the various turbulent zones which effectively delineate the shear zones. In the cross-sections (not illustrated), these zones follow the bedform

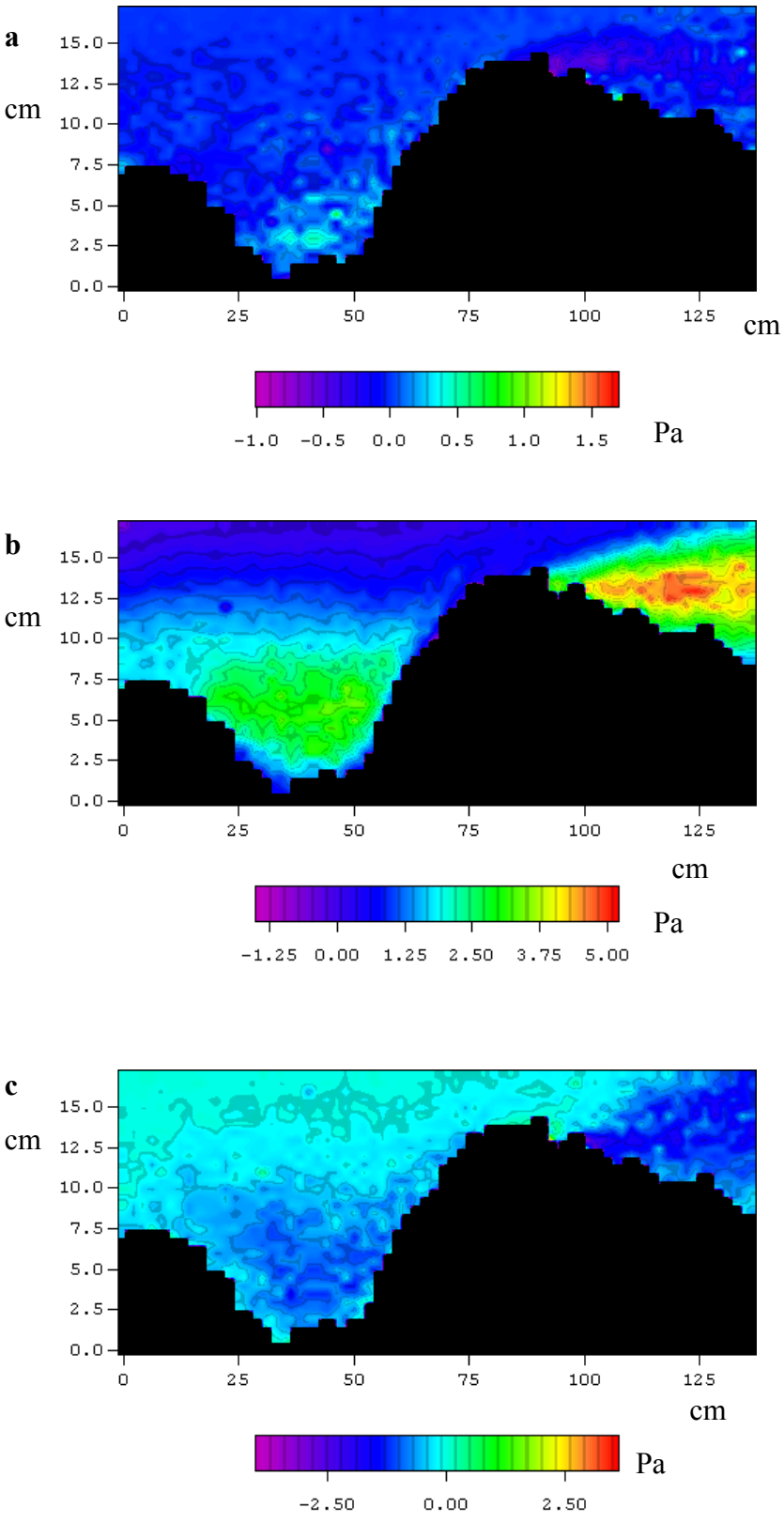

Figure 3.5 The Reynolds stresses present. These are given perpendicular to the *x*, b) *y* and c) *z* directions (referred to as Re_x, Re_y and Re_z respectively).

topography closely. The highest values of the vertical velocity variation are within the pot and between the pot and the tail. In the fourth cross section in each series (near the crest), there are distinct regions of high values of the rms. These are positioned either side of the bedform. These regions exemplify the envelope of turbulence marked out at the crest of the redd extending downstream either side of the topographic high. It should also be noted that the rms values for the cross-streamflow component are particularly high in comparison to the actual velocities. This result tends to suggest that the forcing of the flow in this third lateral dimension is less well defined than in the downstream and vertical dimensions.

The majority of the Reynolds stress (Fig. 3.5) is accounted for perpendicular to the *y* direction. Thus this distribution identifies the same zones of turbulent activity as the root mean square plots. It should be noted that the values recorded in the 3-D case are higher than in the 2-D case. This is because the flow has a greater degree of freedom. The region of high stress is downstream of the crest where there is the additional stress involved with the water coming around the sides of the crest and converging. The values recorded for Re_x are much smaller in magnitude, although they do have the distinction of distinguish different sides of the redd (as this value is closely related to the cross stream velocity.

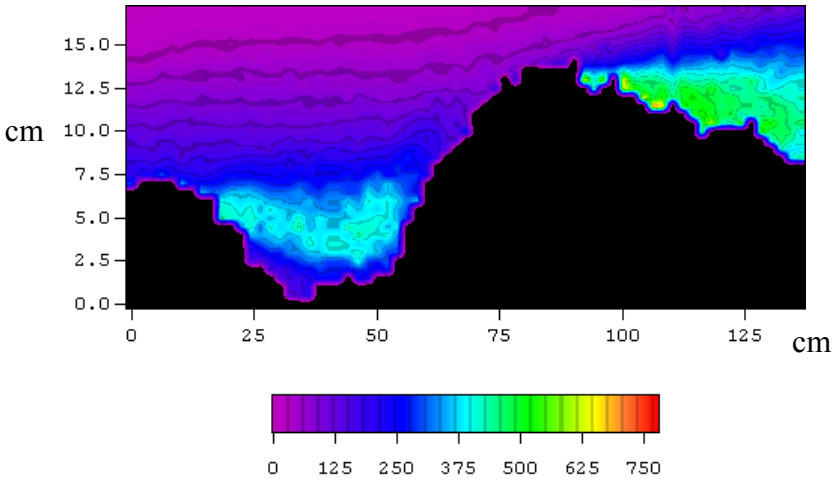

Figure 3.6 Turbulence intensity

Figure 3.6 above, shows the turbulence intensity in the flow. The values shown here are much larger than in the 2-D redd (by a factor of up to 5). In addition, the regions picked out by this characteristic are different in the 3-D run. In the 2-D case, the turbulence intensity was at a maximal value only near the bed. In the 3-D runs, the high values of turbulence intensity pick out approximately the same areas as the rms and Reynolds stress plots. Turbulence intensity increases within the pot but reaches a clear maximum in the lee of the crest of the tail. This is a result of the flow coming round from the sides, which was not possible in 2-D experiment.

3.1.3 Quadrant Analysis and skew values

As in the two-dimensional experiment, a hole value of 2 was used as the threshold value to define a quadrant event. The distributions of quadrant 2 and quadrant 4 events are show in figure 3.7 below.

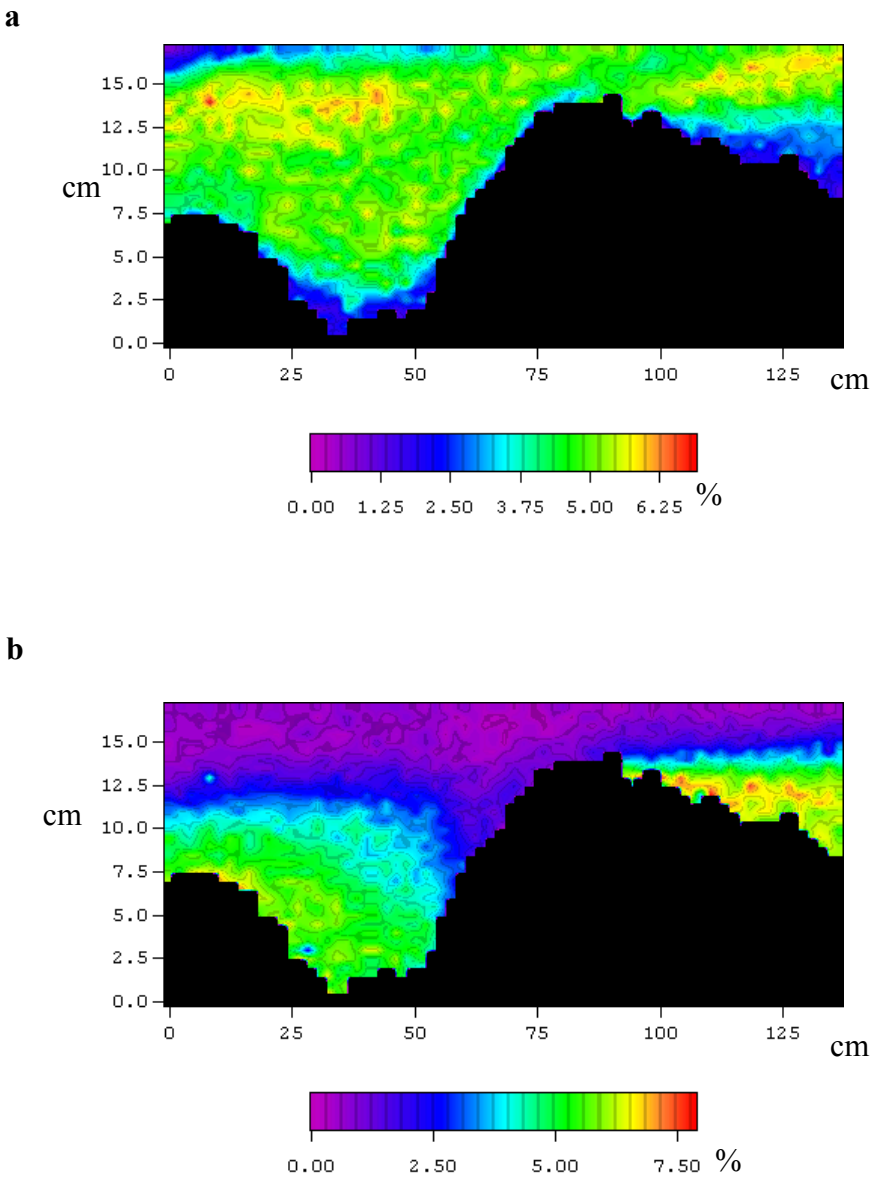

Figure 3.7 Distribution of quadrant events (threshold value of H=2). a) quadrant 2 events; b) quadrant 4 events. Values are given as a percentage of the number of readings.

Quadrant 2 events (sweeps) that is flow 'events' moving towards the bed, are shown to be maximal towards the top of the measured flow (z = 12-15 cm). They are most common just upstream of and above the pot. Another region that shows a high incidence of sweep events can be identified as rising downstream from the crest of the redd. The greatest number of sweep events lies in a region just above or at the roof of the most turbulent area identified in the previous plots (figures 4.20-22). This result is consistent with the notion that quadrant two events usually signify motion from high momentum to low momentum fluid. The quadrant 4 events (or ejections – from low momentum to high momentum flow), are flow events moving away from the bed, and are plotted in figure 3.7b. These are concentrated near the bed and also pick out the low momentum regions associated with the more turbulent parts of the flow. The main region with a high incidence of ejection events is that downstream of the crest. In comparison with earlier diagrams, the zone picked out is within and below the turbulent region. The number of quadrant 2 and quadrant 4 events are comparable to

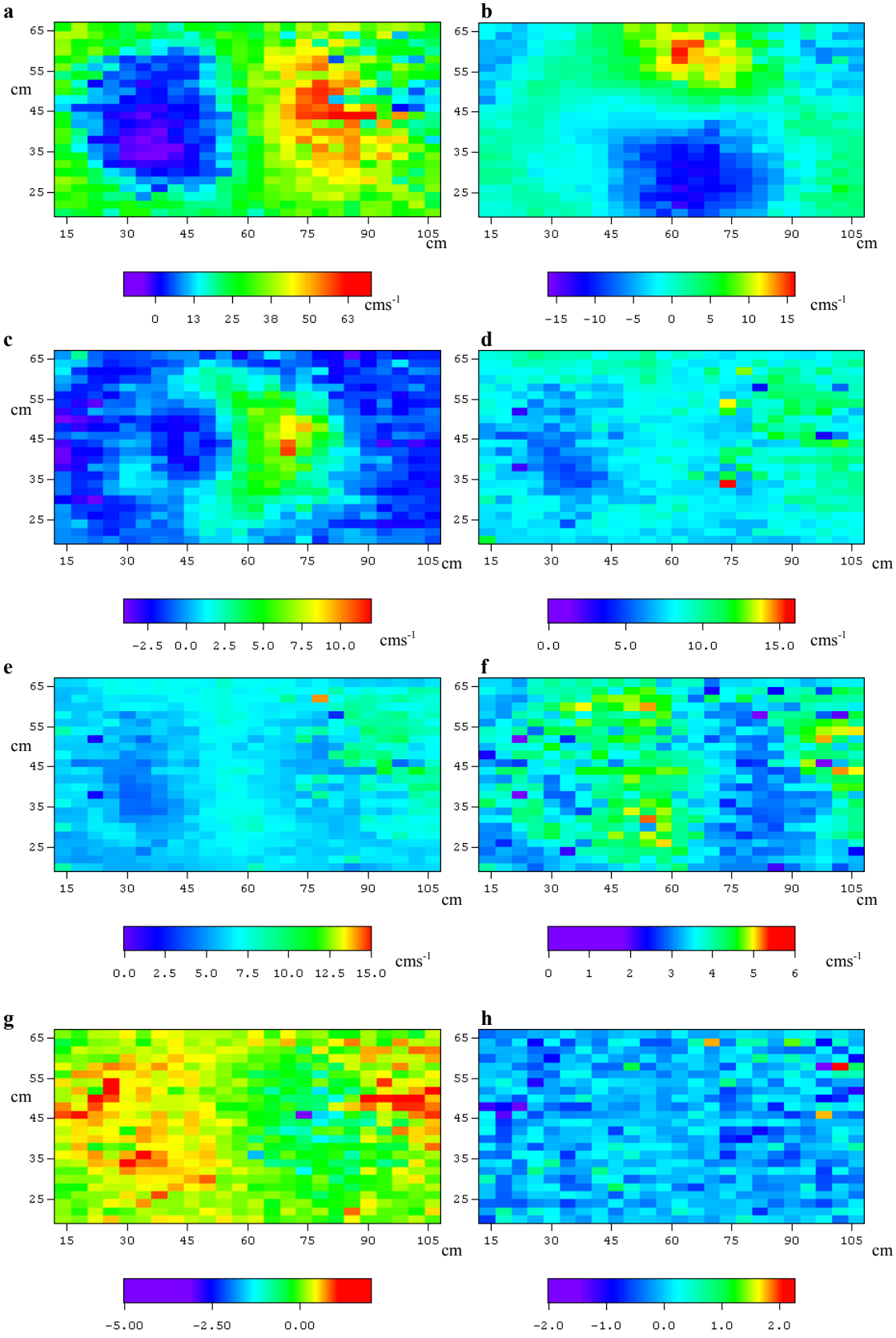
a
b
c
d
e
f
g
h
cm
cms-1
65
55
45
35
25
15
30
45
60
75
90
105
0 13 25 38 50 63
-15 -10 -5 0 5 10 15
-2.5 0.0 2.5 5.0 7.5 10.0
0.0 5.0 10.0 15.0
0.0 2.5 5.0 7.5 10.0 12.5 15.0
0 1 2 3 4 5 6
-5.00 -2.50 0.00
-2.0 -1.0 0.0 1.0 2.0

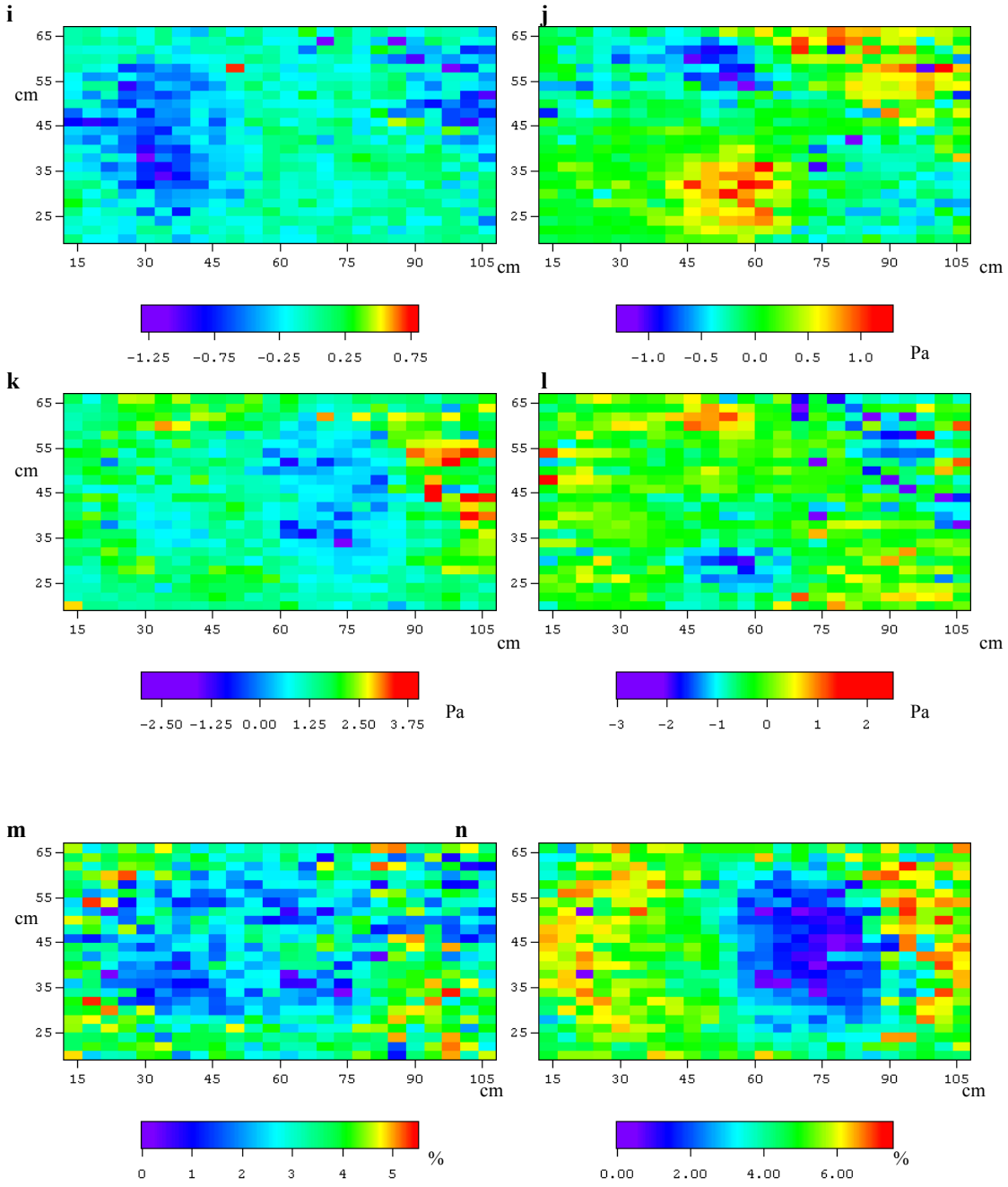

Figure 3.8 Near bed conditions. The axes shown are *x* (left to right) and *y* (bottom to top) with units shown in cm. The plots are a) downstream velocity; b) cross stream velocity; c) vertical velocity; d) u_{rms}; e) v_{rms}; f) w_{rms}; g) skew u; h) skew v; i) skew w; j) Reynolds stress perpendicular to the *x* axis; k) Reynolds stress perpendicular to the *y* axis; l) Reynolds stress perpendicular to the *z* axis; m) proportion of quadrant 2 events; and n) proportion of quadrant 4 events.

the values found in the 2-D investigation. Other aspects of the detail of turbulence are reported fully by Taylor (2000).

3.1.4 Near bed flow

Figure 3.8 shows the values of certain flow parameters near to the bed. The values given are taken from points as close to the bed as possible while still allowing the ADV to record reliable data points. For consistency the data presented are taken from approximately 10mm above the bed. The plots presented in Figure 3.8 are plan views following the bed contours– i.e. they are not horizontal slices of data.

Generally, these plots reinforce the interpretation of data already shown. However, as the data in the near bed region are the most important with respect to interstitial flow models, it should be examined closely. The downstream velocity data shows remarkably fast flow over the crest of the redd, especially along the central axis. A region of reversed flow can be identified (centred on x = 35 cm, y = 35 cm approximately) – just upstream of the base of the pot. The cross-stream velocity closely picks out the topographic forcing of the flow – into the pot from the sides, out of the sides of the pot (around the sides of the crest) with re-attachment occurring further downstream. This is shown clearly in a vector plot. The vertical velocity shows how strong the negative flow is at the base of the pot and that strong upward flow occurs along the downstream wall of the pot (from approximately half way across the pot – x > 45 cm). The region identified in Figure 3.3 as being of reversed flow can also be identified as a region of upward flow surrounded by downward flow.

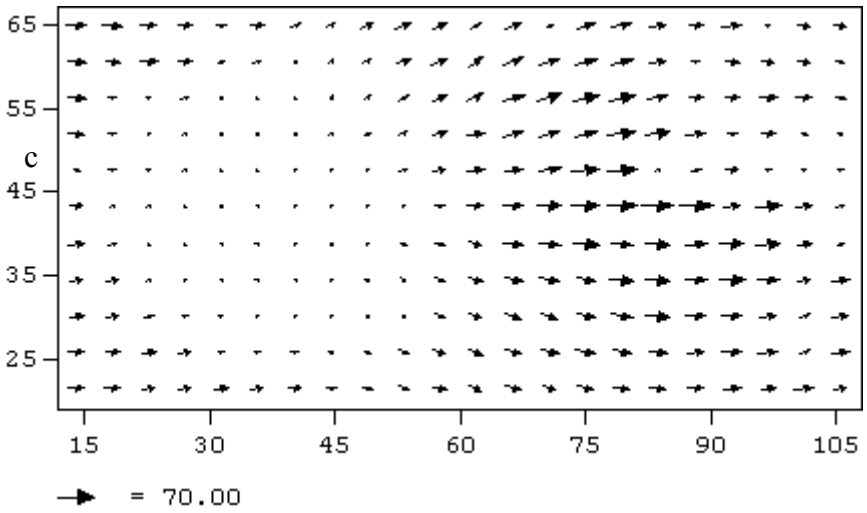

Figure 3.9 Vector plot of the information presented in plot 3.8. The scale arrow shows the velocity in cms^{-1}.

The root mean square plots of the downstream and cross-stream velocities show that the flow at the base of the pot is relatively steady and that on the downstream face of the tail is more variable. The rms values for the vertical flow show a different pattern. The maximum values for this latter case are found along the lip of the pot – particularly along the sidewalls (which coincides with the area in which the vertical flow crosses over from negative to positive flow). The downstream end of the pot and over the crest has particularly low values, showing that the vertical flow in these areas is relatively constant.

The plot of the skew of the downstream velocity shows that forward pulsing is most common downstream of the crest and at the upstream end of the pot. In these areas,

the flow goes from a relatively fast stream into a region that is relatively sheltered and thus is of low velocity. Negative skew results occur just upstream of the crest/downstream of the pot, which suggests that the flow is fast and is being retarded. The negative skew in this area is notably large (approaching -5 at one point), which indicates that the retardation is significant. This region corresponds to the point where the flow drives into the redd structure.

The most significant regions in the Reynolds stress plots are the regions along the sidewalls of the pot and along the sidewalls of the tail. These are picked out in the plots of the Reynolds stress perpendicular to x and z, which suggests that the variation in the cross-stream direction is a major factor. The plot of quadrant 2 events shows that the regions with the highest number of events are around the redd and to a certain extent along its boundaries. The plot of quadrant 4 events shows a much clearer pattern. This latter plot picks out large numbers of events along the upstream end of the pot (and around the pot margins to approximately x = 45 cm) and again downstream of the crest. Quadrant 4 events are usually associated with ejections of low momentum fluid which is in accord with the low velocities found in the pot and downstream of the crest. Conversely, the high velocity region at the pot/tail crossover and over the crest yields a very low number of quadrant 4 incidents.

3.2 Intragravel Flow

3.2.1 Dye visualization

Intragravel flow lines in flat gravel and through the 2-D redd were sketched through the glass side-wall and from video (Figure 3.10).

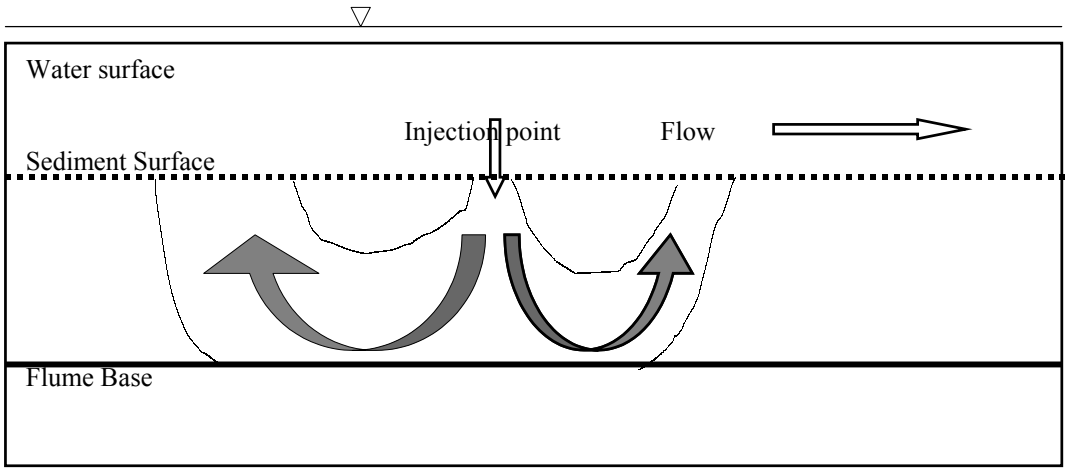

Figure 3.10 Schematic representation of intragravel flow in a flat gravel bed

The direction and strength of intragravel flow is a function of pressure variations at the top of the bed. Circulating cells occur in flat-bedded sediment. For example for a flat gravel bed 130mm thick with 100mm deep flow and flow velocity of 0.76m s^{-1}, dye was repeatedly introduced at a number of points 5mm below the sediment surface. The dye plume descended to the base of the flume and then flowed back to the surface at a speed of 10mm s^{-1} as two arcs, both upstream and downstream, exiting from the gravel surface into the water column some 130mm upstream or

downstream of the injection point. This result demonstrates that there is no strong downslope intragravel flow in the gravel bed, rather dye pumped into the bed returns to the gravel surface largely by diffusion. Evidently it requires topographic variation in the bed surface to induce strong intragravel flow.

In this respect the presence of the redd topography radically altered the intragravel flow pattern through a flat bed. Figure 3.11 is a qualitative depiction of the flow directions recorded in the gravel substrate of the redd. The flow field is similar to that depicted by Thibodeaux & Boyle (1987). The basic circulating cells that occur in flat-bedded sediment may be seen sketched at the far left. However the strength and direction of reverse flow in the bed is a function of the pressure variations at the top of the bed induced by the topographic forcing. Viewing the flow in longitudinal section with the stream flow going to the right, there are two basic cells that can be identified. These two dominant cells diverge around the deepest point of the pot, with one clockwise cell moving upstream towards the left and an anti-clockwise cell moving downstream to the right. There is little intragravel flow penetration directly downwards at the base of the pot. The two large cells are larger, and the flow faster, when compared with the cells found in the flat bed gravel. The downward dimension of the large cells is controlled, in part, by the depth of the permeable layer. However varying the thickness of the bed layer did not alter the longitudinal dimension of the cells. This result reflects the control exerted by the redd geometry on the pressure differentials along the top of the sediment layer. Several small re-circulation cells could also be identified but these were of local significance only. The other salient feature is the angle between the cells - in a flat bed, a downstream sequence of essentially identical cells converge or diverge along vertical 'boundaries'. In the redd, the boundaries are at an angle of up to 45º from the vertical reflecting the control of the redd-distorted flow field in the stream inducing high pressure in the vicinity of the downstream side of the pot. In Figure 3.11 the thin arrows show the general direction of dye tracks. The broad arrows between pecked lines show the direction and width of diffusion of one dye trace injected at point A in the base of the pot. Notably intragravel flow is forced downwards and in a downstream direction through the region of egg pockets. The dye plume diverged downstream of the redd tail, with one plume reaching the gravel surface in a region of low pressure near point B and another flowing further downstream following the base of the flume. The short recurved arrows in the vicinity of point B demonstrate that dye injected at this point is prevented from penetrating the bed owing to the dominance of up welling.

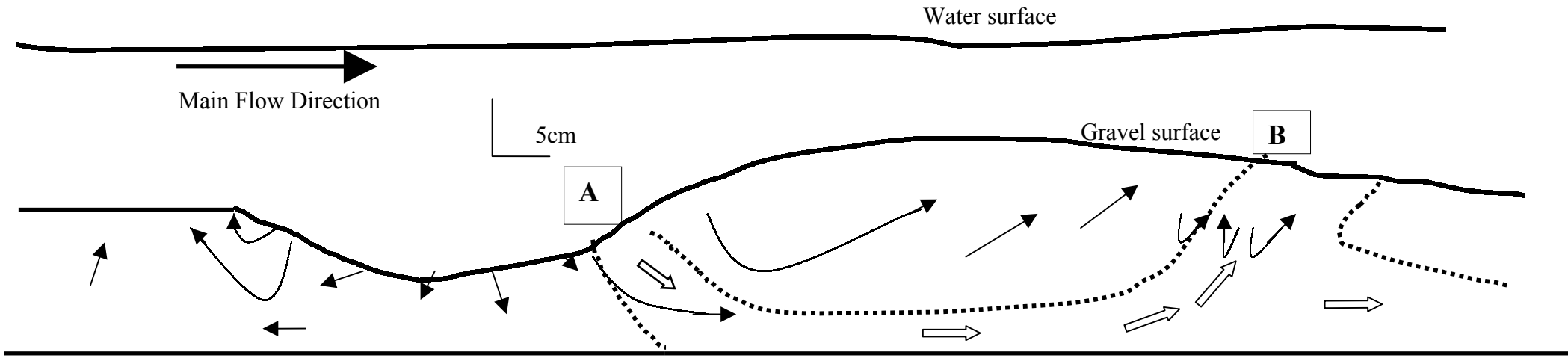

Figure 3.11 Internal flow patterns in the redd. The size of the arrows *does not* represent the velocity of flow

3.2.2 Passive dye detection

The water surface and bed profiles during two typical runs along the centreline of the redd are shown in Figure 3.12. The points at x=2.5m are upstream of the redd, the bottom of the 'pot' is at x=3.4cm and the top of the tail is at x=3.9cm. The locations of groups of detectors during the uniform concentration run are also plotted on the figure as points.

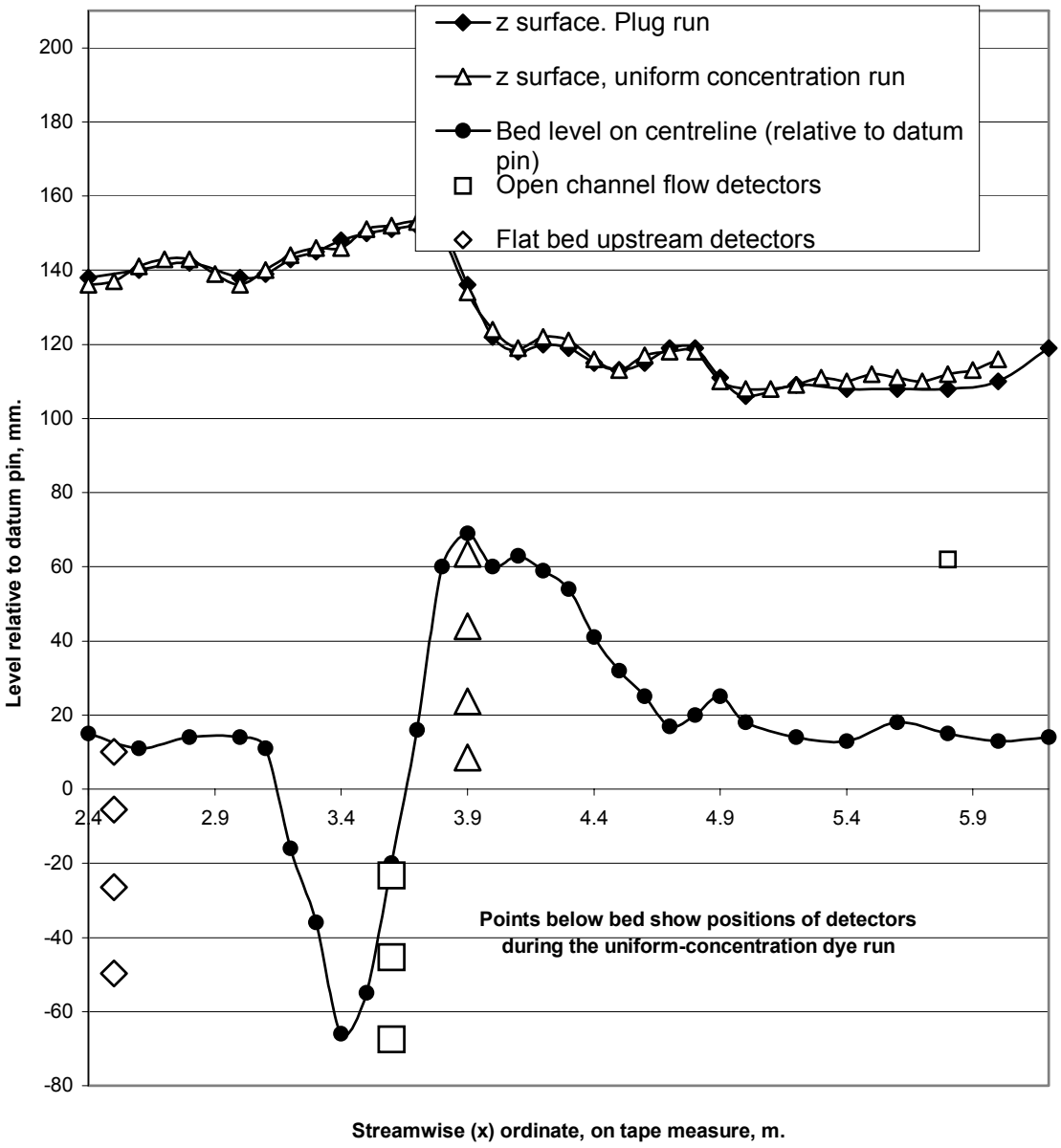

Figure 3.12 Water and sediment surface profiles along moulded redd centreline

In the plug injection run all the groups of detectors were in the surface layer of gravel. The results of the dye extractions after the plug injection are shown in Figure 3.13. The data show an increase in the mixing between main flow and intragravel flow in the region of the redd; about four times as much dye was recovered from the detectors on the tail of the redd than those upstream of the redd. The region of increased mixing appears to persist to some extent downstream of the redd tail. Note that the detectors placed in the main flow did not absorb measurably more dye than those on the tail.

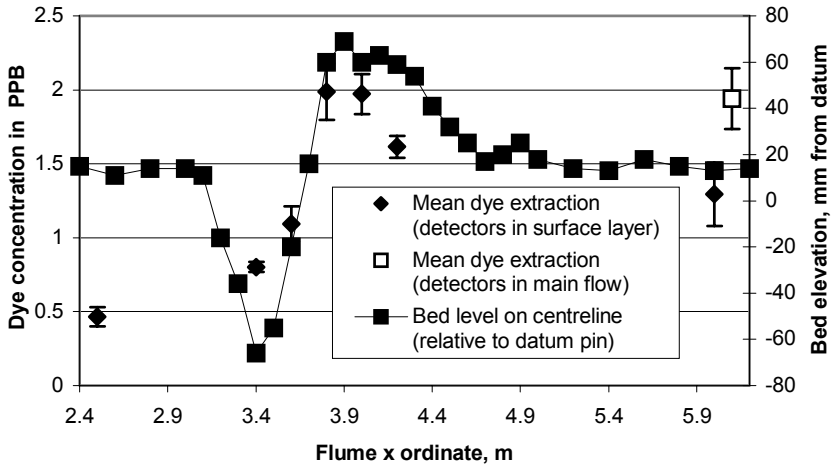

Figure 3.13 Dye extraction from the detectors after the 'plug' injection run (all detectors on the surface of the bed)

The results of the uniform concentration run are presented in Figure 3.14. Dye extraction is on the 'x' axis in the figure. Even 60mm below the bed the increased intragravel flow in the redd tail has produced a strong effect, with nearly twice as much dye being extracted from detectors there than those at a similar depth in the flat bed upstream. Once again, the detectors in the main stream flow did not absorb especially high amounts of dye.

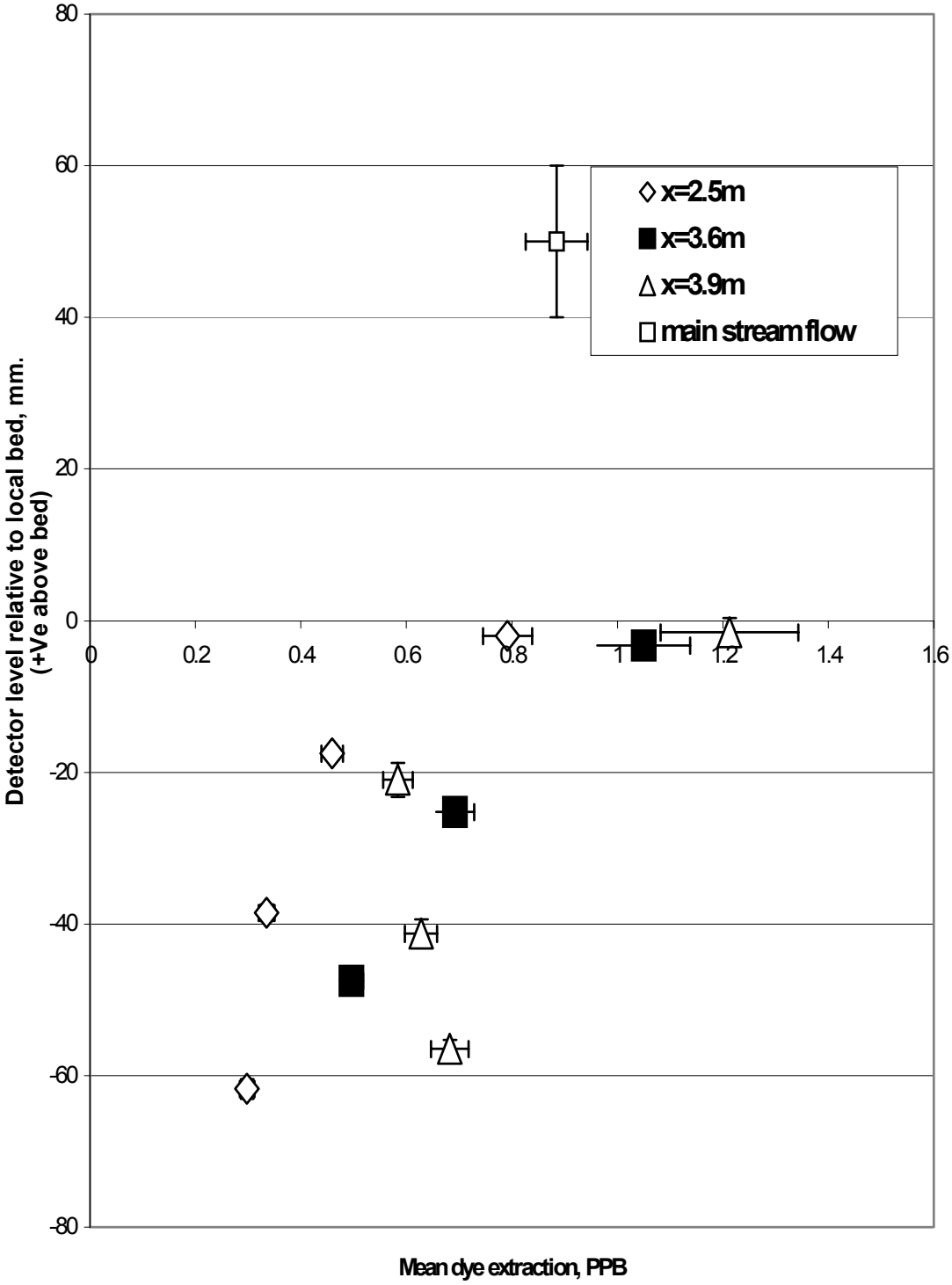

Figure 3.14 Dye extractions from detectors after the uniform concentration run

Earlier results (not illustrated) are in good qualitative agreement with Figures 3.13 and 3.14. These earlier results were from similar experiments in the flume obtained whilst testing the dye tracing technique and used a redd of slightly less amplitude, but otherwise with similar shape and flow conditions.

3.2.3 Determination of experimental error in the dye extraction results

The dye extraction results from each group of four detectors were treated as a sample of a statistical population. The sample mean was used as an unbiased estimator of the population mean for detectors at that location. However, with only four data points in each sample, a direct estimate of the standard error in the population mean would have been a very weak estimate. Instead, it was supposed that the error in the population mean would be related to the population mean in a simple way, and the results for each group of four detectors was plotted as a point on a graph of these variables. An exponential fit matched the points well (Figure 3.15). In addition it made good sense, since some error is predicted even with a mean of zero which at 0.007PPB is comparable to the noise on the fluorimeter. This exponential fit was used to determine the error bounds in dye extraction concentration for each mean result.

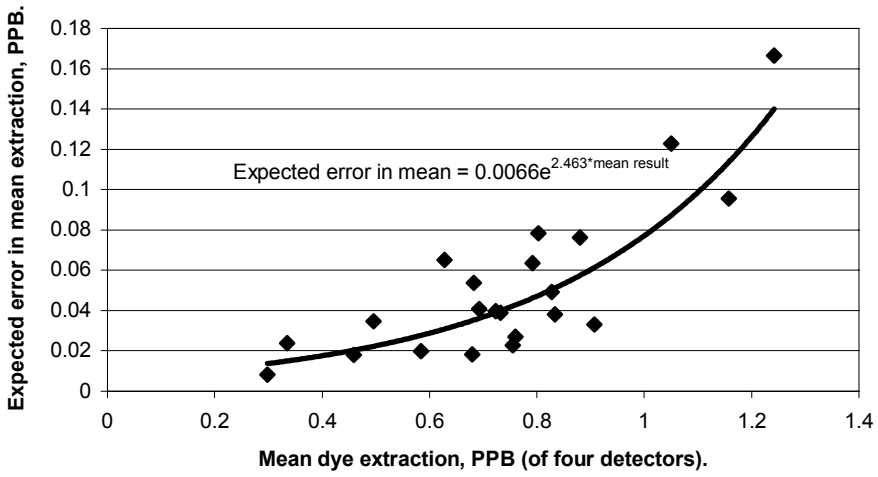

Figure 3.15 Analysis of variance in the dye extraction results

3.2.4 The linearity of dye accumulation in the detectors over time

Figure 3.16 shows the results of detectors sequentially removed from the flume during the uniform concentration run; the error bars are double those seen earlier since the sample size was n=1 rather than n=4. These detectors evidently absorbed dye at a steady rate and there was no evidence of detector saturation up to 0.5PPB Rhodamine in the extraction solution.

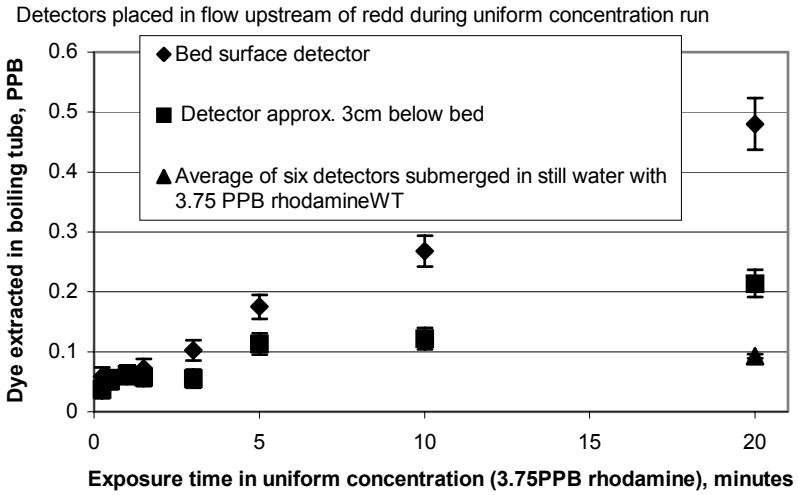

Figure 3.16 Dye extracted against detector exposure time

3.2.5 The saturation of detectors with dye or contaminants

Saturation of the detectors at equivalent to around 1parts per billion Rhodamine in the extraction solution is the obvious explanation for another observation: the results obtained from detectors in the free-stream flow did not greatly exceed those of detectors placed in even the 'best' areas of the tail. There are two objections to this dye saturation explanation though:

1. In favourable locations the detectors in the bed surface layer could adsorb more dye than the free-stream detectors (from the data in Figure 3.15 there is a 90% chance this result is significant, and this result is supported by data from an earlier experiment (not illustrated).

2. A few individual detector results were as high as 3PPB in the dye extraction solution, especially in one preliminary experiment with a similar dye concentration in the flume and a much longer duration to the uniform concentration run.

Two possible alternative explanations for the low results of the free-stream detectors are offered:

1. It is a genuine effect; i.e. that the average dye concentration gradient at the charcoal surface is similar for detectors placed in the main flow or in the exposed areas of the tail.

2. A tentative explanation only: there may be contaminants in the flume water which are able to replace the Rhodamine in the charcoal; the greater the exposure of a detector in terms of flow velocity and time, the greater are the number of active sites in the charcoal that are 'poisoned'. Thus, there is a certain degree of exposure that yields maximum Rhodamine concentration in the detector; increasing the exposure beyond this level only allows the contaminant to remove dye.

3.3 SIDO-UK Model

All the changes given in Table 7.1 (Appendix) were implemented, and three scenarios to represent different hydrographs and antecedent conditions were investigated as given in Table 3.2 below.

Table 3.2 Different SIDO modelling scenarios

Scenario	Hydrograph and suspended sediment record	Fish size and redd angle	Result figures	CBAD J	Purpose for investigating
A	Base flow	45.5cm/ 14.3	Fig. 3.18, 3.19,etc	1	Mean for GEB storm flow: 30 mg/l (Carling ,1983)But 3mg/l for a base flow
B	Fig. 2.4	45.5cm/ 14.3	Fig. 3.23, 3.24,etc	1	All Northern UK upland information – with flashy hydrograph. Peak S.S. load also representative of pollution incident
C	Fig 2.4	45.5cm/ 14.3	Fig. 3.29, 3.30,etc	1/50	As above, but using SIDO example redd composition

3.3.1 Scenario A

Here the average quantities from the Lune site are used, such as the mean temperature (8.3^{o} C) and average discharge. The base flow suspended sediment load is used. Comparisons are also made between species for this scenario, where possible. The 'verification' table from SIDO has been divided into a set of graphs which now follow.

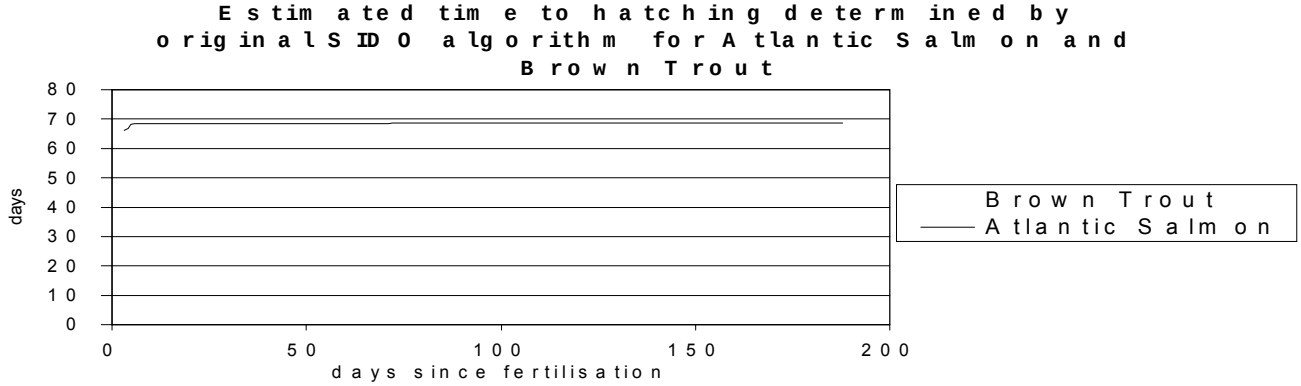

Figure 3.17 Estimated time to hatching determined by the original SIDO algorithm for Atlantic salmon and brown trout

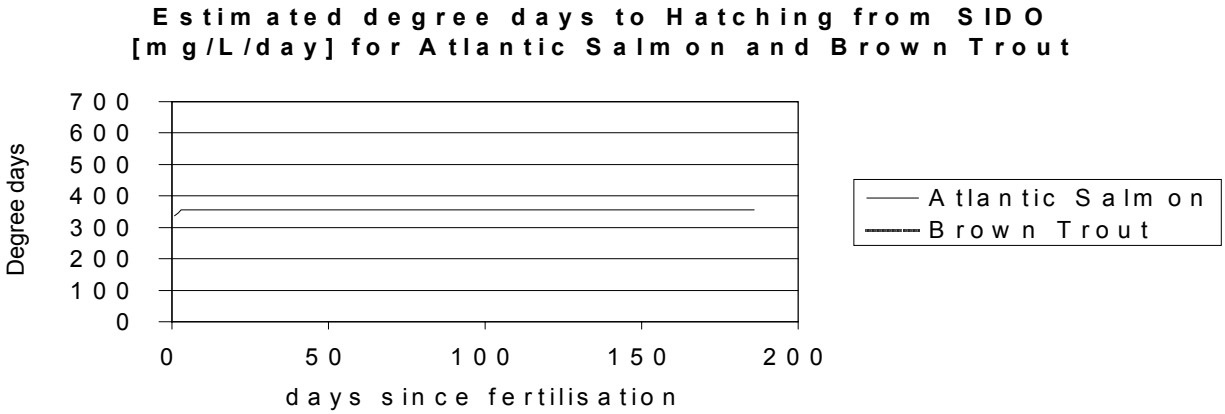

Figure 3.18 Estimated degree days to hatching from SIDO for Atlantic salmon and brown trout

The number of degree days for the average flow conditions have been investigated for comparison with other observations. SIDO predicts degree days to hatching as Atlantic salmon 353 and brown trout 573 degree days, which compare to the 444 degree days for 50% alevin hatching determined by Elliot for brown trout . Using the Hamor and Garside algorithm, the estimated hatching time reaches a plateau of 34.5 days, corresponding to 288 degree days for brown trout. This algorithm specifically relates to the 50% hatching rate, whereas it is not clear from the literature as to what percentage the SIDO algorithm relates to.

However, the Hamor and Garside formula also predicts an excessively long hatching time for Atlantic salmon (>1000 days). This could be due to a number of factors, including the fact that the intragravel pore space, the dissolved oxygen concentration in the substrate and the flow rate are all smaller for the Atlantic salmon, by factors of 0.67, 0.5 and 0.1 respectively. Since these quantities are not vastly different between the species, it would appear that the Hamor and Garside algorithm can be very sensitive, and it appears to be the flow rate which is mainly responsible for the sensitivity. More investigations need to made into whether the hatching rate would really be affected so drastically by these changes. Later (scenario B) it is strongly evident that the larger predicted hatching times for slow flow rates are more realistic than the existing SIDO algorithm.

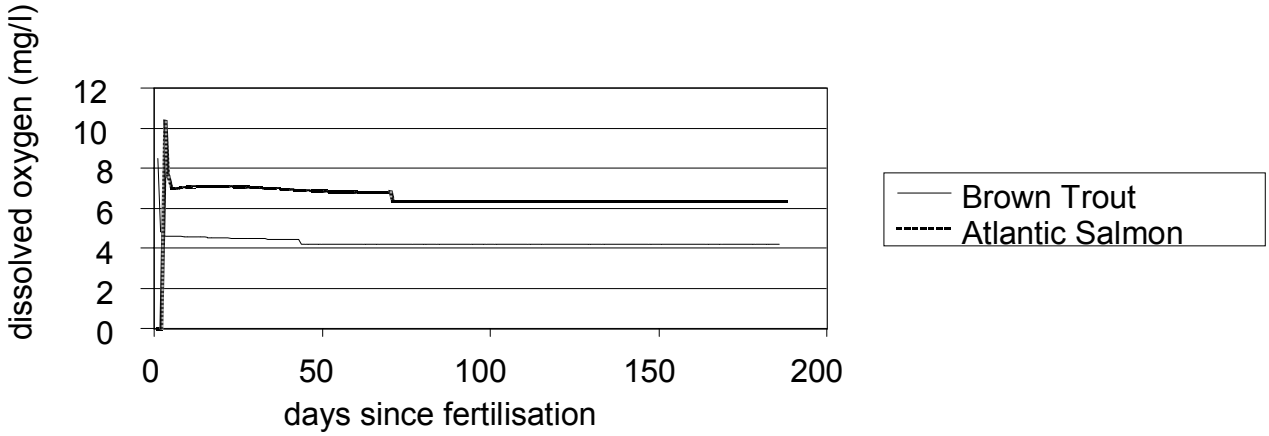

Figure 3.19 Dissolved oxygen as calculated by SIDO for Atlantic salmon and brown trout

Figure 3.19 shows that the predicted dissolved oxygen remains approximately within the range given by Carling (1985) of 5-13mg/l for embryo survival, although the level for brown trout is slightly low.

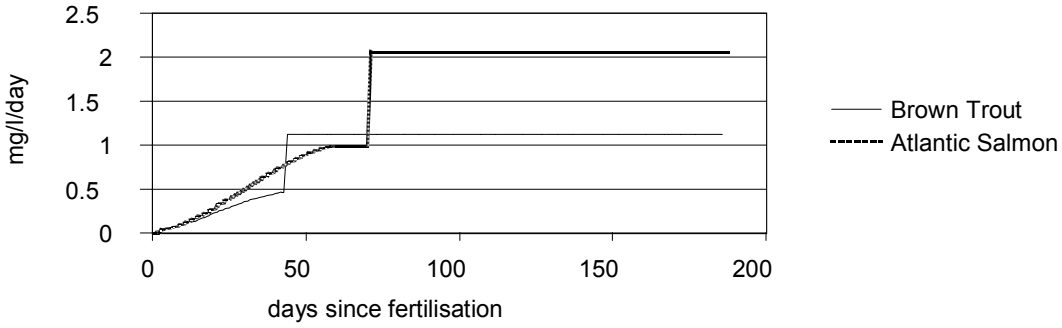

Figure 3.20 Egg oxygen consumption predicted by SIDO for Atlantic salmon and brown trout

Figure 3.20 is for unit volume of interstitial water volume. Carling (1985) cites a critical threshold for embryo survival for Brown Trout as 0.0036 to 0.014 mg egg^{-1} hr^{-1}, and although it is not clear how to compare this with the above units, there are approximately 10 eggs per litre of egg zone, so a value of 2 mg l^{-1} day^{-1} translates to 0.003 mg egg^{-1} $hour^{-1}$, if we take into account average porosity of the egg zone, which is near the lower end of the ranges of concentrations for survival.

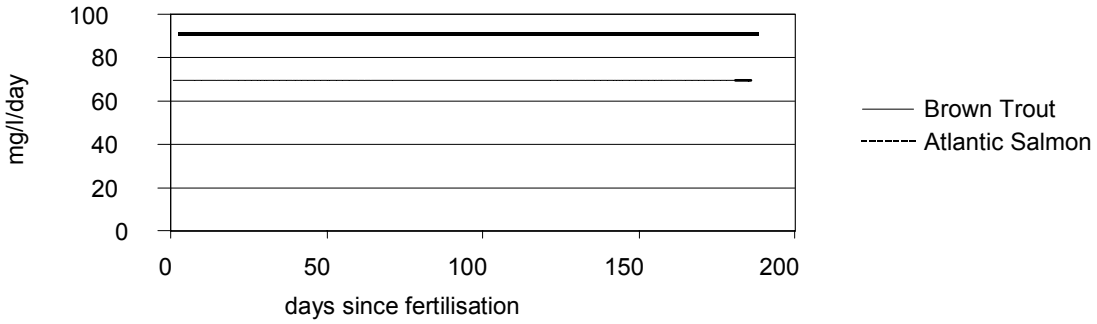

Figure 3.21 Percentage fry emergence predicted by SIDO for Atlantic salmon and brown trout

The percentage fry emergence (Fig. 3.21) appears to be reasonable, although the algorithm used, as discussed earlier, is considered to be unreliable.

3.3.2 Scenario B

Scenario B uses the 186 day hydrograph and suspended sediment concentrations given in Figure 2.5. All of the time-variable information for the Lune site is used, in conjunction with the various physical and biological parameters discussed in sections 1-3, the values of which are given in the Appendix.

Blocking status, siltation and porosity.

The redd pit fills through the modelled bed-load transport process on day 33 after the first large flood event, and remains filled with sediment thereafter, with a porosity of 0.33 in the pit. The consequences that follow the siltation process can be seen in the graphs below. A porosity of less than 0.13 gives problems for hatching, whilst a porosity in the range 0.24-0.30 is clean, and values of around 0.41 or larger implies 'over loose' after a flood (Carling, unpublished). The grain size of the material filling the redd gives rise to a porosity of 0.33, so the oxygen concentration should remain at levels that are sufficient for continued survival of the eggs. However, figure B1 indicates otherwise, and could be explained by the concurrent siltation process which appears to reduce the flow rate and oxygen supply. Carling and McCahon (1985) found that:

'Trout redds are likely to be fully silted in 2-3 days under flow regimes subject to small freshets with an adequate supply of fines', which suggests that the predicted scenario is not unrealistic.

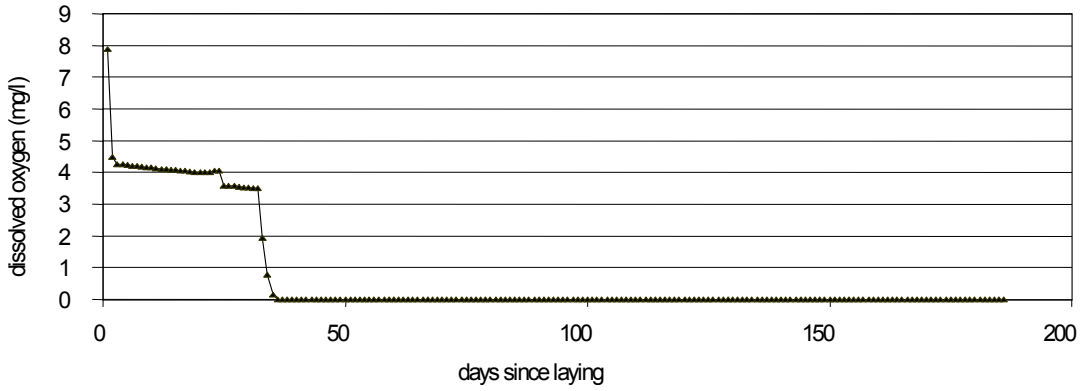

Figure 3.22 Dissolved oxygen as calculated by SIDO (mg l^{-1})

The estimated time to hatching is given in two further graphs: Figure 3.23, based on equation 1b, which does not account for drop in flow rate; and fig. 3.24 based on equation 2, which does account for the drop in the inflow rate that occurs on day 33. Day 33 corresponds to the redd filling up with fine sediment, owing to a large discharge and consequent sediment load. This was discussed earlier with reference to Table 3.2, and it would appear that the Hamor and Garside equation is more realistic under these circumstances.

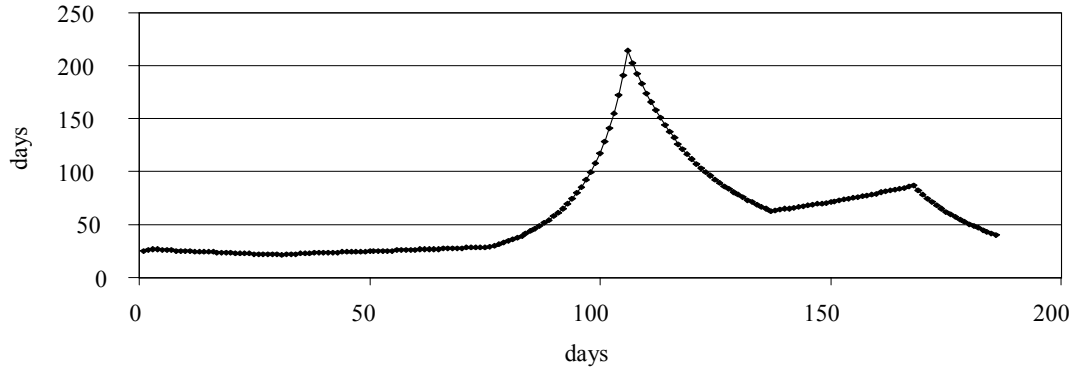

Figure 3.23 Estimated time to hatching using original SIDO algorithm

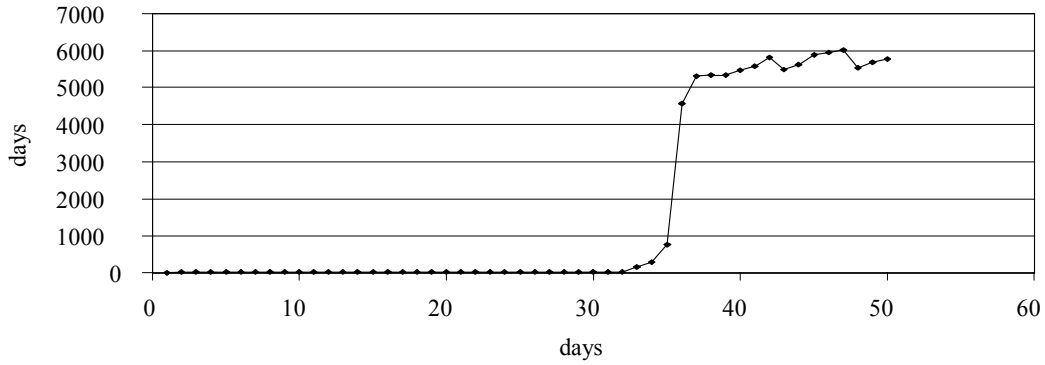

Figure 3.24 Estimated hatching time for fertilized eggs using Hamor and Garside algorithm

Figure 3.24 is more 'realistic', because the predicted dissolved oxygen level drops to zero (Fig. 3.20), well beyond the range given by Carling (1985) of 5-13mg/l for embryo survival, such that the eggs will never hatch and the predicted hatching time goes towards infinity.

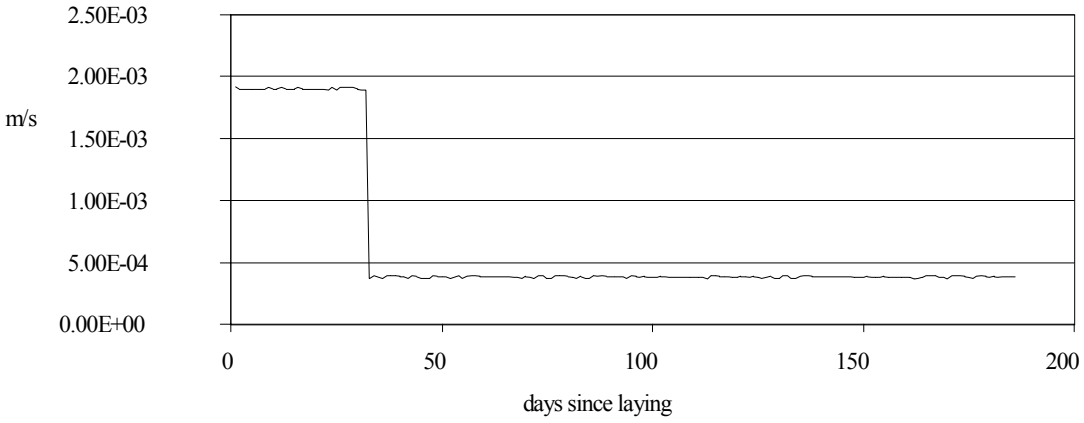

Figure 3.25 Intragravel velocity determined by SIDO

The impact of redd siltation on the quantity of water flowing past the eggs is illustrated in Figure 3.25, and it can be seen that there is a radical reduction in flow following the large flood event after 33 days. This kind of response could equally well represent the effect of an anthropogenically induced sediment pollution event on a redd. The mean interstitial velocities reduce to the order of 1 cm hr^{-1}, which compare with the lowest in the range of intragravel seepage velocities measured by Carling (1985), of between 1-1000cm hr^{-1} – where the lowest were recorded at heavily silted sites.

Figure 3.26 indicates the predicted oxygen consumption, which cannot be met by the supply (see Fig. 3.22), and consequently the predicted fry emergence would be expected to decline rapidly (Fig. 3.27).

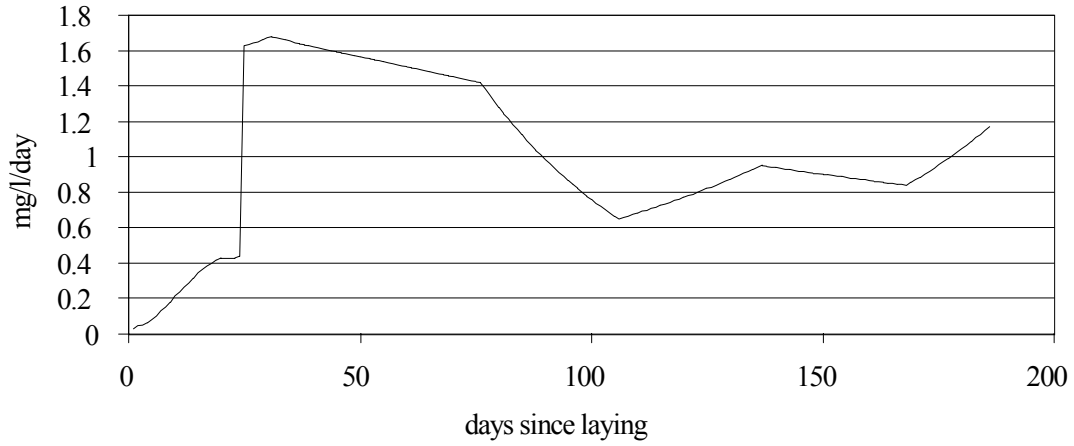

Figure 3.26 Egg oxygen consumption predicted by SIDO (mg $l^{-1}day^{-1}$)

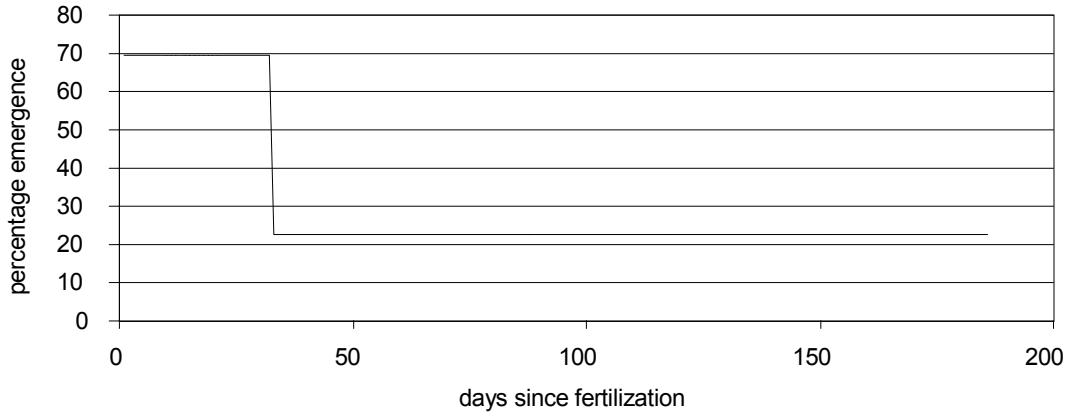

Figure 3.27 Predicted fry emergence from SIDO

Fry emergence is initially predicted at just under 70%, which departs from the figure of 96% for recently cut redds in the US study. This is probably owing to the finer composition of the redd for the UK situation (the UK composition is taken from Crisp and Carling, 1989, see Appendix 1), although the species differences should be considered. The effect of the sediment-laden peak flow after a month is clearly to block up the intragravel pore spaces and reduce the flow and oxygen supply to the eggs, reducing percentage fry emergence, although one would expect this to reduce to zero give apparently lethal DO contents in the gravel.

3.3.3 Scenario C

Scenario C uses the 186 day hydrograph and suspended sediment concentrations given in figures 2a and 2b. However, it also uses the substrate material that was used in the American example, given as the original values in Table 7.1 of the Appendix. For this example there is less very fine material in the original bed material immediately before eggs are deposited. This results in the redd remaining unblocked for longer, ultimately predicting a greater proportion of fry to emerge, as might be expected.

Apart from the first period for which the velocity is given, the velocities in Table 3.3 are compatible with those measured at the spawning grounds in Crisp and Carling (1989), where the measured flow velocities at 0.6 of the depth ($U_{0.6}$) were in the range:

$0.15ms^{-1} < U_{0.6} <$ (2*body length) m s^{-1}

which for the average fish length investigated here is :

$0.15m\ s^{-1} < U_{0.6} < 0.9m\ s^{-1}$.

Because the flow velocity at 0.6 depth is typically taken to be approximately the depth-averaged velocity, the predicted flow velocities for the engineered reach represent values that are realistic for spawning grounds.

Table 3.3 Blocking / filling status over 186 day period, CBADJ=1

```
Filling Statu
     [ O = pass-thru cell,  F = filling cell,  B = Blocked ce
     Day = 184                                        CBADJ =
     O  O  O  O  O  O  O  O  O  O  O  O  O  O  O  F  B  B  B  B  B  B  B  B  B  B  B
     F  O  O  O  O  O  O  O  O  O  O  O  O  O  O  O  B  B  B  B  B  B  B  B  B  B  B
     B  O  O  O  O  O  O  O  O  O  O  O  O  O  O  F  B  B  B  B  B  B  B  B  B  B  B
     B  O  O  O  O  O  O  O  O  O  O  O  O  O  O  B  B  B  B  B  B  B  B  B  B  B  B
     B  F  O  O  O  O  O  O  O  O  O  O  O  O  O  F  B  B  B  B  B  B  B  B  B  B  B
     B  B  O  O  O  O  O  O  O  O  O  O  O  O  O  B  B  B  B  B  B  B  B  B  B  B  B
     B  B  O  O  O  O  O  O  O  O  O  O  O  O  F  B  B  B  B  B  B  B  B  B  B  B  B
     B  B  F  O  O  O  O  O  O  O  O  O  O  B  B  B  B  B  B  B  B  B  B  B  B  B  B
     B  B  B  O  O  O  O  O  O  O  O  O  F  B  B  B  B  B  B  B  B  B  B  B  B  B  B
     B  B  B  F  O  O  O  O  O  O  O  F  B  B  B  B  B  B  B  B  B  B  B  B  B  B  B
     B  B  B  B  F  O  O  O  O  O  O  F  B  B  B  B  B  B  B  B  B  B  B  B  B  B  B
     B  B  B  B  B  F  O  O  O  F  B  B  B  B  B  B  B  B  B  B  B  B  B  B  B  B  B
     B  B  B  B  B  B  F  F  F  B  B  B  B  B  B  B  B  B  B  B  B  B  B  B  B  B  B
     B  B  B  B  B  B  B  B  B  B  B  B  B  B  B  B  B  B  B  B  B  B  B  B  B  B  B
     B  B  B  B  B  B  B  B  B  B  B  B  B  B  B  B  B  B  B  B  B  B  B  B  B  B  B
     B  B  B  B  B  B  B  B  B  B  B  B  B  B  B  B  B  B  B  B  B  B  B  B  B  B  B
     B  B  B  B  B  B  B  B  B  B  B  B  B  B  B  B  B  B  B  B  B  B  B  B  B  B  B
     B  B  B  B  B  B  B  B  B  B  B  B  B  B  B  B  B  B  B  B  B  B  B  B  B  B  B
```

Table 3.4 Blocking / filling status over 186 day period, CBADJ=50

```
     FILLING STATU
     [ O = pass-thru cell,  F = filling cell,  B = Blocked cel
     Day = 184                                      CBADJ = 5

     O  O  O  O  O  O  O  O  O  O  O  O  O  O  B  B  B  B  B  B  B  B  B  B  B  B  B  1
     F  O  O  O  O  O  O  O  O  O  O  O  O  O  F  B  B  B  B  B  B  B  B  B  B  B  B  1
     B  O  O  O  O  O  O  O  O  O  O  O  O  O  B  B  B  B  B  B  B  B  B  B  B  B  B  1
     B  O  O  O  O  O  O  O  O  O  O  O  O  F  B  B  B  B  B  B  B  B  B  B  B  B  B  1
     B  F  O  O  O  O  O  O  O  O  O  F  B  B  B  B  B  B  B  B  B  B  B  B  B  B  B  1
     B  B  O  O  O  O  O  O  O  O  F  B  B  B  B  B  B  B  B  B  B  B  B  B  B  B  B  1
     B  B  O  O  O  O  O  O  O  F  B  B  B  B  B  B  B  B  B  B  B  B  B  B  B  B  B  1
     B  B  F  O  O  O  O  O  O  B  B  B  B  B  B  B  B  B  B  B  B  B  B  B  B  B  B  1
     B  B  B  O  O  O  O  O  O  B  B  B  B  B  B  B  B  B  B  B  B  B  B  B  B  B  B  1
     B  B  B  F  O  O  O  O  O  B  B  B  B  B  B  B  B  B  B  B  B  B  B  B  B  B  B  1
     B  B  B  B  F  O  O  O  F  B  B  B  B  B  B  B  B  B  B  B  B  B  B  B  B  B  B  1
     B  B  B  B  B  F  O  O  B  B  B  B  B  B  B  B  B  B  B  B  B  B  B  B  B  B  B  1
     B  B  B  B  B  B  F  F  B  B  B  B  B  B  B  B  B  B  B  B  B  B  B  B  B  B  B  1
     B  B  B  B  B  B  B  B  B  B  B  B  B  B  B  B  B  B  B  B  B  B  B  B  B  B  B  1
     B  B  B  B  B  B  B  B  B  B  B  B  B  B  B  B  B  B  B  B  B  B  B  B  B  B  B  1
     B  B  B  B  B  B  B  B  B  B  B  B  B  B  B  B  B  B  B  B  B  B  B  B  B  B  B  1
     B  B  B  B  B  B  B  B  B  B  B  B  B  B  B  B  B  B  B  B  B  B  B  B  B  B  B  1
     B  B  B  B  B  B  B  B  B  B  B  B  B  B  B  B  B  B  B  B  B  B  B  B  B  B  B  1
```

Table 3.5 Hydraulic conditions for Scenario C

Sect. No.	Distance [m]	Top Width [m]	Hydr. Depth [m]	Flow Area [sq.m.]	Froude Number [-]	Hydr. Radius [m]	Flow Velocity [mps]	Water Surface [m]	Thalweg Elev. [m]	Comp. N-value [m]	Flow Depth [m]	Normal Depth [m]	Critical Depth [m]
Day 46 Hydraulics Table--discharge = 4694.00 [ls]													
1	0.00	9.76	0.5290	5.16	0.3958	0.4718	0.9013	6.2081	5.5800	0.0315	0.6281	0.6281	0.3700
2	200.00	9.87	0.5093	5.03	0.4141	0.4764	0.9254	6.7069	6.1000	0.0330	0.6069	0.7488	0.3557
Day 92 Hydraulics Table--discharge = 1436.00 [ls]													
1	0.00	9.24	0.4066	3.76	0.1897	0.3815	0.3788	6.0656	5.5800	0.0465	0.4856	0.4856	0.1888
2	200.00	9.22	0.3432	3.16	0.2452	0.3041	0.4499	6.5045	6.1000	0.0473	0.4045	0.5301	0.1922
Day 138 Hydraulics Table--discharge = 2351.00 [ls]													
1	0.00	9.44	0.4578	4.32	0.2544	0.3967	0.5391	6.1237	5.5800	0.0381	0.5437	0.5437	0.2493
2	200.00	9.46	0.4072	3.85	0.3027	0.3686	0.6048	6.5793	6.1000	0.0407	0.4793	0.6100	0.2444
Day 184 Hydraulics Table--discharge = 1760.00 [ls]													
1	0.00	9.31	0.4277	3.98	0.2139	0.3660	0.4380	6.0895	5.5800	0.0411	0.5095	0.5095	0.2112
2	200.00	9.31	0.3688	3.43	0.2671	0.3296	0.5078	6.5339	6.1000	0.0445	0.4339	0.5610	0.2116

The SIDO model has a coefficient CBADJ, that controls the ratio of near bed suspended sediment to substrate sediment concentration, which is varied in the American study in order to control the over all rate of infilling. The rate of in-filling is very dependent on the stream velocity and the factor CBADJ. If the mean stream velocity is increased to 0.9 m s^{-1} the cells begin to fill rapidly. Thus the model can be calibrated to match the observed infilling rate for sites that are studied. The CBADJ factor was left at unity for scenario A, since we it was considered that through using the Rouse equation, the near bed suspended sediment concentration was known. However, in order to demonstrate its effect, CBADJ is now increased from 1 to 50 (50 is the value used in the SIDO example), giving rise to an increase in the rate of infilling and the blocking of cells in Table 3.4 compared with Table 3.3.

Silt distribution in redd

The silt distribution fluctuates from day to day between 0.01 to 0.04 % mass per volume, but remains reasonable uniform in the pot for this scenario. This results in the effective porosity remaining at 0.33 in the base of the pot.

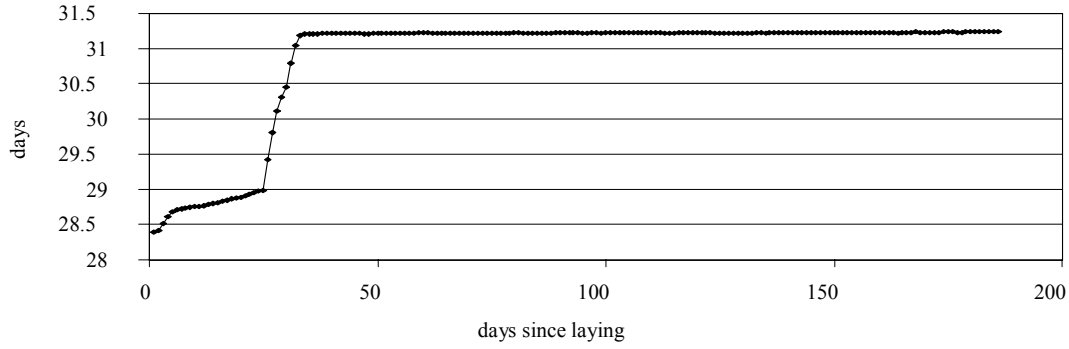

Figure 3.28 Estimated time to hatching for eggs determined by original SIDO algorithm

Following the large flood event after the first month, the conditions remain relatively stable, in terms of oxygen concentration (albeit rather low – see Figure 3.29 below), which is the principal variable apart from temperature that effects the estimated time to hatching. If the Hamor and Garside algorithm is used, then the estimated hatching time also reaches a plateau, this time at 35 days (rather than 31 days) as in Figure 3.38 above. The similarity between these indicates that for scenario C, the flow rate is not dramatically altered as in scenario B, and its omission is therefore more justified for cases where the redd composition is coarser. However, this assumes that the suspended sediment load is mainly composed of silt.

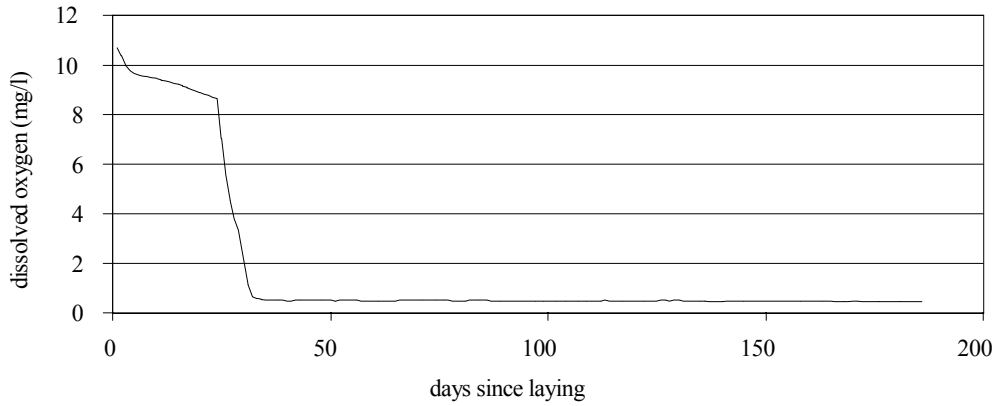

Figure 3.29 Dissolved oxygen as calculated by SIDO (mg l^{-1})

The effect of the sedimentation for this scenario suggests, that using the coarser substrate material affords greater availability of oxygen, and larger flow rates (Fig. 3.30), which both contribute to the survival of more of the embryos. However, it is clear that sediment-laden peaks of this magnitude present difficult conditions for survival. The slow reduction in percentage emergence of fry in figure C5 after the first flood peak should be attributed to the slow filling of the pot (Table 3.4) rather than the slight oxygen deficit that can be seen between calculated dissolved oxygen and predicted oxygen demand (compare Figures 3.29 and 3.31 to observe this deficit). This is because, as already discussed, the fry emergence algorithm in SIDO is independent of oxygen levels.

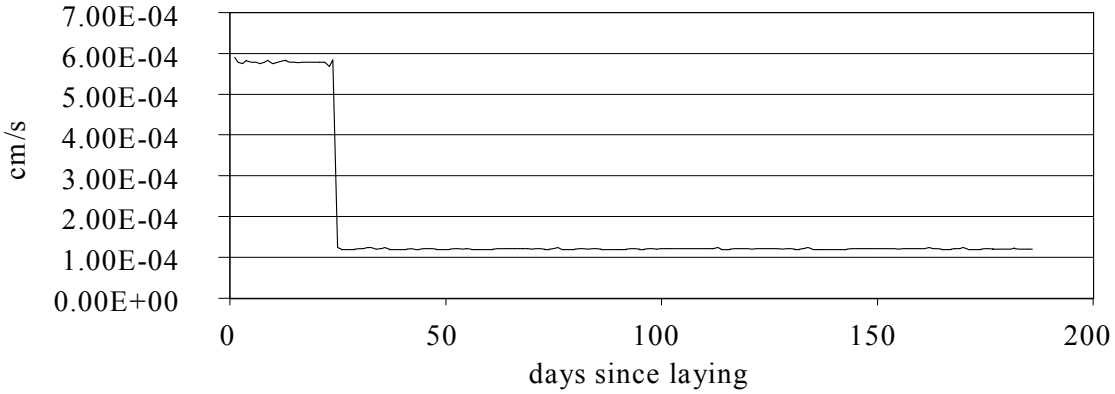

Figure 3.30 Intragravel velocity determined by SIDO

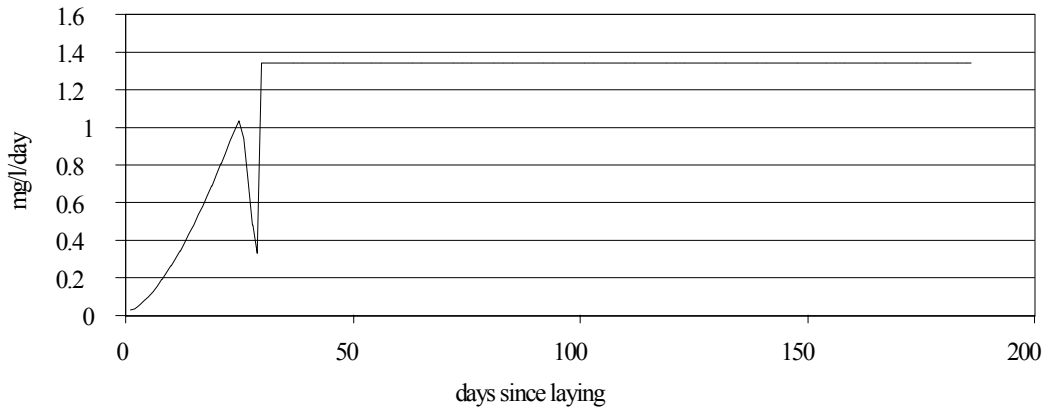

Figure 3.31 Egg oxygen consumption predicted by SIDO (mg l^{-1} day^{-1})

4 DISCUSSION

4.1 Turbulent Flow

One of the more important points is the significance of the difference between the two-dimensional and three-dimensional experiments.

4.1.1 Two-dimensional experiment

Simplifying the problem to two dimensions allows comparison with earlier studies such as Bennett & Best (1995). Full graphic presentation of the 2-D results are to be found in Taylor (2000), here only the main pertinent points are discussed. The flow field is superficial similar to that shown in Fig. 3.3 but there is a larger element of flow forcing in the 2-D case is evident in the distribution – this is particularly evident at the pot/tail crossover (at x = 50 - 60 cm). It is also evident downstream of the crest where the flow is forced downwards. At the upstream end of the pot (x = 0 – 20 cm and z < 5 cm) the flow is near stagnant. This zone is separated from the main flow and does not seem to be affected by it. There is a distinct separation evident in more detailed flow information. At point *b*, the separation between the regimes is at a height of approximately 6 cm. There is a similar separation downstream of the crest at a height of 10 cm. In both cases, these areas are characterised by the bedforms. At these points, the bedform dips downwards at relatively high angles. The water downstream and below of these features can be considered separately from the main flow. These regions are effectively shielded from the flow and are low velocity in nature. Flow within these regions is due to interaction over the upper surface of the lower body of water. The result of interaction between a fast and a slow moving body of water is a high degree of variation in the velocities recorded. Momentum is transferred between the two bodies in a turbulent fashion. As a result of this, the separation between the zones was highlighted in plots of the root mean square, quadrant event frequency, and the Reynolds stress.

The root mean square plots show maximal values in regions that correspond with the proposed zones of separation. This is consistent with the hypothesis of separation. The region of high values does extend vertically. The maximal values delineate a region approximately 10mm thick, but high values surround this up to a thickness of 80mm in the pot and 50mm above the tail. This demonstrates the extent of the disturbance caused by the interaction between the regions of high and low flow. The angles at which the zones rise (3.5º downstream from the crest and 7.2º within and above the pot) suggest angles at which vortices, generated along the shear zone rise. The Reynolds stresses demonstrate similar regions to those picked out by the root mean square plots.

The vertical velocity of the vortices can be estimated from these plots. The calculation is based on the angle at which the upper end of the zone (defined by high root mean square values) rises downstream and the downstream velocities measured at that point. This gives a range of values. Within the pot, the value calculated is of the order of 3 cm s^{-1}. Downstream of the crest the velocity is of the order of 2.5cm s^{-1}. The vertical flow velocity downstream of the crest is of the order of 1 cms^{-1}. The values within the pot vary considerably, but at the points where the angle was

measured the value is near zero. Correcting for the vertical velocity, the rate at which vortices rise to the surface is consistent for two the two different areas. Examining the quadrant event plots does not yield particularly good information on the separation between the high velocity and low velocity zones. However, these plots do allow further characterisation of the zones. The upper, faster zone is defined by a high rate of incidence of quadrant 2 events and a low rate of incidence of quadrant 4 events. Conversely, the low momentum fluid demonstrates a large number of quadrant 4 events and a low number of quadrant 2 events. Quadrant 2 events (sweeps) are pulses directed forwards and downwards. This pulse is faster than the mean flow velocity at that point (by definition) and therefore represents a transfer from high momentum to low momentum flow. Similarly, a quadrant 4 event (ejection) is slower than the mean flow field and therefore represents a transfer from low momentum to high momentum flow.

The skew values of $\boldsymbol{u}$ and $\boldsymbol{w}$ give additional information on the pulsing of flow. While quadrant event plots give an indication of the number of events, the skew values combine the number and strength of the pulses. The regions outlined by the skew plots are the same as those in the quadrant event plots. The plot of Reynolds stress shows a distinct layer between the highly turbulent areas downstream and upstream of the crest. This region is marked by a low value of Reynolds stress. This is one of the clearest indicators of the degree of separation caused by the flow over the crest. The turbulence intensity plot is biased towards low velocities and it is therefore difficult to extract useful information on the flow structure around the redd. As already demonstrated, the turbulence intensity measurement is biased towards regions of low velocity. However, it is still possible to delineate the region downstream of the crest picked out by the root mean square plot. The high values recorded within the pot ($x = 0 – 40$ cm and $z < 5$ cm) are of low priority.

4.1.2 First three-dimensional experiment

Most flow studies have concentrated on examining the flow properties in a limited, two-dimensional fashion. Now that the technology is available to study flows in three dimensions simultaneously, it is important to extend experiments to utilise this ability. The redd is a very distinct three-dimensional bedform. Simply reducing the problem to two dimensions ignores much of the physical processes occurring. The two-dimensional flow demonstrates similarities with the three dimensional experiment. The plots which show the flow along the central plane of the redd (figure 4.15) have many elements in common. However, there are critical differences. Firstly, there is a region of reversed flow on the upstream end of the pot. This is more evident in the 2-D case. The two bodies of water (the main flow and the body in the pot) are separate and the upper body drives the motion of the lower one. In this case, the force has been sufficient to initiate a recirculation cell within the pot. The reason for this difference between the two-dimensional and three-dimensional is not altogether clear and requires further experimentation.

The flow velocities at the upstream end of the pot are similar, but not identical. At 5 cm above the bed at point *a*, the flow velocity in the 2-D case is 43 cm s^{-1} compared with 49 cm s^{-1} for the 3-D case (values are given to two significant figures). The angle α is slightly greater in the 3-D case (23.6º as compared with 20.1º). The differences in these two factors, flow speed and angle of entry into the pot, when

comparing 2-D and 3-D results do not seem to be sufficient to produce the stronger separation in the 2-D case. More likely the increased lateral freedom of flow in the 3-D case is responsible for the weaker flow separation. Examining the cross sectional diagrams of the flow (not shown in this report) illustrate that this is a reasonable assumption. The diagrams (at x = 38 cm – i.e. within the pot), demonstrate that in the 3-D case the flowlines near the bed spiral into the pot with sub-parrallel rollers developing and converging on the central axis of the pot, the left-hand roller spiralling clock-wise and vice-versa. However this motion is quickly transformed into diverging rollers which dissipate above the exit slope from the pot. In contrast in the 2-D case, the flow is constrained by the walls of the tank and a distinct transverse roller develops similar to a classic flow separation downstream of a negative step. Another major difference between the mean flow field (as demonstrated along the central plane of the redd) is that there is a much greater variation in the vertical velocities measured. Although the downstream velocities are of the same order of magnitude, the vertical velocities measured in the three-dimensional experiment have a much higher range than that recorded in the two-dimensional experiment. Again, the reasons for this are unclear.

The high values of V were recorded at the crossover point between the pot and the tail (at x = 60 cm). Therefore, the higher values of V might be expected if the value of β was significantly higher in the three-dimensional experiment (as the flow forcing should be more apparent). This is not the case as the angle β measured 29.9º in the 2-D experiment and 21.8º in the first 3-D case. Indeed, Figure 4.1 demonstrates that the forcing of the flow is such that the flow is forced round as well as over the tail crest. The velocity profiles at point c in both experiments allows an easy comparison. In the two-dimensional case, the maximum vertical velocity is 6.8 cms^{-1} at a height of 0.8 cm above the bed. In the three-dimensional data set, the vertical velocity reaches 7.9cm s^{-1} directly above the bed. The downstream velocity at these points measures 42.4 and 38.7 cm s^{-1} respectively. This evidence shows that the higher vertical velocity is not simply a feature of a faster flow in the area. The most reasonable explanation of this phenomenon is that the flow at the downstream end of the pot converges as it follows the wall of the pot round. This flow would then be forced upwards at the base of the downstream wall of the pot. However, at the third cross section, the flow is shown to diverge around again (see figure 5.1).

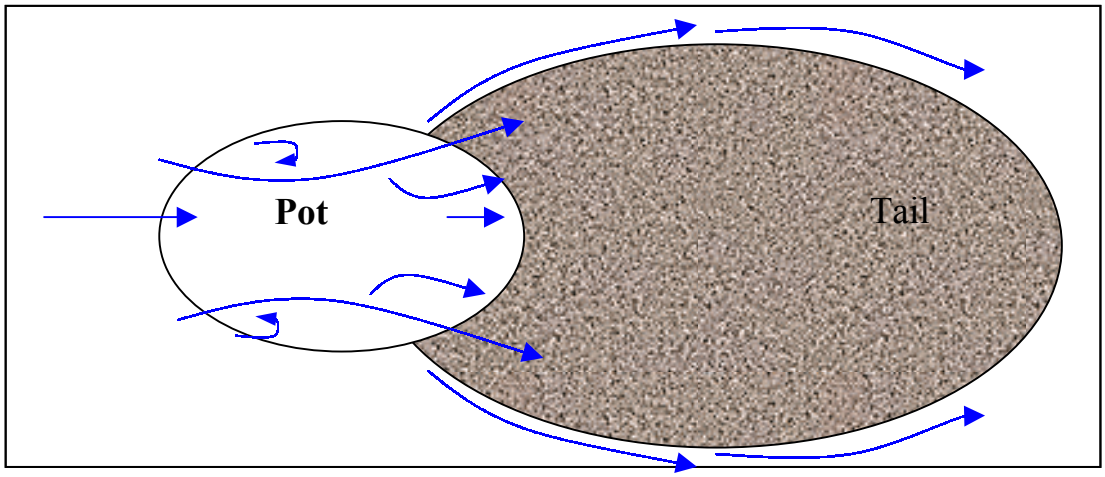

Figure 4.1 Flow pathways in plan view around the pot and tail

Finally, on the point of the mean flow field, in the 3-D case the flow field starts to "recover" from the effect of the redd within the sampling grid. This is much faster than the recovery downstream of the redd in the 2-D experiment. This is simply due to the greater freedom of the flow (i.e. it is not restricted by the proximity of the flume walls).

The root mean square plots show analogous regions of shear to those in the two-dimensional experiment. The three-dimensional sampling method allows the complete shape of the shear zone to be delineated. The clearest shear zone (located downstream of the crest) clings to the shape of the tail. The shape of the affected volume is similar to that displayed for horseshoe vortices as shown in figure 3.4 albeit with a different type of vortices. The height of the shear zone is much greater along the central axis of the redd than at any other point along the cross section. This is because the shape of the bedform offers greatest resistance to the flow along this downstream pathway. It should also be noted that the lower boundary of the highly turbulent region is approximately horizontal (as opposed to the two dimensional data where the zone was near parallel to the bed). This is because the equilibrium of the flow can be restored by flow parallel to the *y*-axis. The region of high rms in the pot is a more complex shape. Again, the zone clings to the bedform. There is a small area close to the bed at the upstream end of the pot (x = 20-40cm) which essentially forms a recirculation cell. This is distinct from the high rms zone above it. The zone has the greatest vertical extent along the central plane and above the side-walls of the pot.

Using the same method as described above it is possible to estimate the vertical velocity of the eddies shed from the two main shear zones. Details on the zone near the pot are difficult to determine, as the structure does not yield clear linear features. The lower boundary has been used for calculations, although this is not an ideal selection. The angle at which this zone rises is 19º and the downstream velocity at the point measured is 40cm s^{-1}, yielding the rate at which the vortices rise from this area as approximately 13.8cm s^{-1}. The upper boundary of the shear zone originating from the crest of the redd is much better defined. The angle measured here was approximately 4.2º. Combined with the downstream velocity at this point of 60cm s^{-1}, this yields an estimate of 4.9cms^{-1} vertically for the shedding vortices. The vertical flow velocities at these points are approximately 5 and –4 cm s^{-1} respectively. Hence, the corrected rates at which the vortices rise are similar in both cases. However, the velocity yielded in this experiment is more than double that recorded in the two dimensional experiment.

The quadrant event plots demonstrate the same factors as those in the two-dimensional experiment. The quadrant 2 events are distinctive of the high momentum zone and the quadrant 4 are characteristic of the low momentum zone. What is important to note is that the area with a high number of quadrant 2 events is not as extensive in the three-dimensional as it is in the two-dimensional. In particular, the region towards the top of the measured flow upstream of the pot and the near-bed region downstream of the crest have a low incidence of quadrant 2 events. The region near the bed with a low quadrant 2 event incidence has a near horizontal upper boundary. This reinforces the separation between the flow bodies demonstrated in the root mean square plots.

Also of great interest is a plot of the quadrant 2 events on the cross section across the tail. This image picks out the same region as the rms plot. However, in addition over the top of this region there is a region of low incidence of quadrant 2 events. Further above this low region is another higher region which demonstrates a high zone of quadrant 2 incidence. This sandwich layer with a low incidence of events is difficult to explain. The most reasonable rationalisation is that the low layer is of no significance. The "high" region below it is a result of the flow separation and the high values above it are simply due to the recovery of the flow to a high velocity.

Skew values of the velocity demonstrate the same regions of separation as shown in the figures already discussed. Extremely negative values of skew found near the bed are most likely due to problems of measurement connected with the ADV. The most important area is picked out by a plot of vertical skew values. In addition to the region of high positive skew leading off downstream from the crest of the redd (approximately x = 80 cm +), there is a region of near zero skew which forms a layer above this. This is important as it is linked to the "sandwich" region picked out in the root mean square plots. This suggests that the flow in this region is of low turbulence and unusually steady. This is due to the forcing of the flow by the bedform and demonstrates the extent of the separation.

The turbulence intensity (as shown Fig. 3.6) and the Reynolds stress (Fig. 3.7) plots do not yield any additional information of use in characterising the flow. Although they both mark out the same regions already identified, they offer no new information. In addition, the definition of the areas of interest is poor in these plots.
The near-bed plots are important in defining boundary conditions for interstitial flow models. With respect to the overall flow patterns, the most interesting plot is the root mean square plot of vertical velocity. The high points of this plot occur around x = 45-60 cm at the lips of the pot. This is related to the complexity of the flow within the pot (see above).

4.1.3 Second three-dimensional experiment

Although the second three-dimensional experiment shows many similarities with the previous experiment, there are important differences. In addition, there are several differences in the scale of the measurements. Of the latter, the main differences in the velocity measurements are summarised in Table 3.5. The phenomenon of reversed flow is much clearer in this experiment (with reversed flow of up to $-10 cm^{-1}$). The values recorded in all plots have a greater range of values. This is indicative of a greater degree of turbulence.

One of the main differences between the two three-dimensional experiments is the degree of deformation in the water surface immediately downstream of the crest. However, in comparison with that recorded in the two-dimensional experiment, the deformation occurs at a much higher velocity and recovers at a short distance (approximately 50mm) downstream of the most deformed point. In the two-dimensional flume the recovery of the water surface is limited (the bedform does not vary in the y direction). In addition, the walls of the flume greatly confine flow. Neither of these factors apply to the three-dimensional experiment.

The plots of the root mean square velocities can be used to estimate the upward velocity of the vortices. The results are summarised in table 5.1, below. As can be seen from these results there is a great diversity. The relationship between these velocities is not obvious. The most tenable suggestion is that the velocity depends on the velocity of the main flow and the degrees of freedom in the flow.

Table 4.1 Estimated value of the vertical vortex velocity

	Two-dimensional experiment	**First three-dimensional experiment**	**Second three-dimensional experiment**
Corrected velocity estimate (cm^{-1})	3-3.5	9-10	5-5.3

4.1.4 Other studies

Turbulence studies to date have, by necessity, concentrated on two-dimensional measurements. While this is a justified approach when considering two-dimensional bedforms, it is not possible to validate this when studying three-dimensional structures.

Bennett and Best (1995) described in detail the flow over two-dimensional dunes. The sampling strategy is similar in extent to that used in this study. There are several important differences in the two bedforms (dunes and redds). Firstly, the scale of the two features as studied is different – in the case of the ripples, they measure 40mm high and 63mm long. The redd used however measures approximately 130mm from the lowest point to the highest and 1.3 m long. The faux bed used in the Bennett and Best study is impermeable, such that the entire flow pattern is related simply to the shape of the bed. Also, the redd is a stand alone features whereas the dunes measured were part of a repeating pattern. Finally, the shapes of the two structures are very different.

In order to make useful comparisons between the two studies, the same flow properties were recorded or calculated. Comparing the flow properties on a type by type basis allows the best evaluation of the similarities and differences. Simply examining the mean flow field demonstrates a significant difference. The lee side of the dune crest is characterised by a significant region of flow reversal. In this case the region is comparatively (as compared with the size of the bedform) larger and better defined than the corresponding region at the upstream end of the pot. The reason for the poor definition of the reversed flow in the redd's pot is that the two main negative steps in the topography are in regions that are not particularly well suited. The first negative step (where reversed flow is in evidence), the flow over the top of the step is at a low velocity. At the upstream lip of the pot, the velocity is low, as it is typical of the bottom of a vertical profile for a flat, gravel bed. Downstream of the crest, flow separation and reversal does not occur due to the low angle of the negative topographic slope. In comparison, the reverse flow is well defined in the lee of the dune as the flow in this area is high (a combination of flow forcing and the fact that it is relatively high in the water column). This, combined with the topography (a high angle on the lee slope), ensures the flow separation.

The pattern of reattachment demonstrated in the Bennett and Best study is not closely paralleled in this study. In the case of the redd, the main flow is directed towards the bed surface (at the pot/tail cross over point) at a height comparable with the main bed downstream of the feature. Reattachment within the pot does not occur due to the low velocities that occur. The root mean square plots in the Bennett and Best study demonstrate high values in the lee of the dunes. In the case of the downstream velocity, the rms values are only high below the level of the height of the crest. In addition, the disruption recorded by this parameter disperses quickly, so that it is not clear on the upstream edge of the next dune-form. The scale of the redd in relation to the depth of the flow means that the high rms values (in both the downstream and vertical velocity) dominate high into the flow. The values of the rms of the vertical velocity show are better defined. In this plot, it is possible to distinguish three distinct vertical layers before the flow recovers from the bedform. There is the initial boundary layer, a mixing zone and the unaffected zone above that. The main mixing zone is quite short in extent (mainly dispersed by approximately half way along the bedform). In the case of the redd, these layers show a different pattern. There is a well-established mixing or shear zone downstream of the crest. However, unlike in the case of the dune form, this region is not horizontal but rises significantly into the flow. The mixing zone over the pot is a completely different shape – this is because it is forced into this shape by the topography and low downstream velocity in the area.

The values of the velocity measurements quoted in the Bennett and Best study are of the same order of magnitude as recorded in this study. However, the rms values are higher around the redd than over the dune forms (by a factor of two). This is a result of the roughness elements used. The sediment used in the Bennett and Best study was of sand size as opposed to the gravel used to form the redd. In addition, the roughness element associated with the bedform is much higher in the case of the redd as compared to the dune. Both of these factors combine to give a much higher resistance to flow around the redd than around the dune.

There are important differences in the skew values of the velocities plotted in the two studies. The skew values calculated by Bennett and Best do not display any variation with height, characteristic of the plots in this study. In both studies, the shear zones demonstrate strong positive skew values in the vertical velocity. However, in this study, the high values are also recorded in the upper part of the flow. The reason for the difference is not clear.

High Reynolds stress values are indicative of turbulent activity. Reynolds stress is highly anisotropic with most of the stress accounted for in the plane perpendicular to the *y*-axis. In both this and the Bennett and Best study, high values are recorded in the separation zones. There is a difference of scale however. In the Bennett and Best study, the Reynolds stress reached 9 Pa, whereas the highest value recorded around the redd was of the order of 5 Pa. This is because the degree of separation in the lee of the dune crest is much more defined. The shear layer downstream of the crest of the redd separates a zone of high momentum flow from low momentum flow, but due to the topography involved, the is not sufficient to instigate flow reversal. Hence, despite the higher values of the flow velocity and roughness elements, the value of the Reynolds stress is lower in the case of the redd.

Quadrant analysis depends on the ability to measure flow velocity in two perpendicular directions simultaneously. This is a possibility that has only been realised in the last few years. Quadrant 2 and 4 events dominate the contributions to the Reynolds stress involved. Over the dune, there is a marked zone (the separation layer) which demonstrates a high level of quadrant 2 events. This zone is thin and rises at a low angle. However, the low angle is parallel to the bed below it. In comparison the region of high incidence above the crest of the redd is more of a wedge shape not parallel to the bed. This suggests that this shear zone is less stable with a tendency to oscillate in angle. This is possible in part because the bedform is higher in the flow than in the case of the dune.

4.2 Intragravel Flow

The flow properties were only established to a qualitative standard in the two-dimensional experiment. Comparing figure 4.12 with figure 2.14 and Thibodeaux and Boyle (1987) demonstrates the similarity between this study and previous work. Figure 2.14 is not the result of a redd as a bedform. However, it is possible to draw a parallel between the shape of the redd and the ripple feature used. In this case, the lee side of the ripple is comparable with the lee side of the redd's crest. In both cases, there is a downward step at a significant angle (although the angle is greater in the case of the ripple). Following on from the work by Thibodeaux and Boyle, this suggests that the low pressure on the lee side of a bed feature aids in the pumping of the interstitial flow. In both cases (figures 4.12 and 2.14), the interstitial flow is "drawn" towards the low-pressure regions above the sediment. There is no easy comparison between the situation at the upstream end of the pot and any other common bedform. In this case, there is a significant negative step without a positive step preceding it.

As described in section 2.3, the interstitial flow in the case of a flat bed consists of a number of half-cell re-circulating units (in the two dimensional case). These units are of equal scale (as long as the internal structure of the sediment in statistically similar) and alternate between forward and reversed flow. If the bed deviates in any way, the pattern of half-cells distorts. In this case, one half-cell has elongated to cover the critical part of the redd (from x = 25 cm to x = 90 cm). The half-cells adjacent to the main half-cell are distorted. They are compacted in the x-direction. The main half-cell is distorted at the downstream end. Instead of the more typical vertical division between the half-cells, the boundary is at an angle of approximately 45º. The half-cells downstream of this are at an angle. However, by the third half-cell, the flow structures (although still compressed horizontally) are near vertical, describing some form of lateral recovery.

The experiments were limited to a clean washed gravel, but the dye and activated charcoal detector technique was a useful physical analogue to dissolved oxygen and salmonid eggs. At the start we set out to show that the availability of dissolved oxygen to eggs is increased by the interaction of the redd and the streamflow. The results support this hypothesis. The plug injection run shows that the mixing between the main stream flow (carrying the dye plume) and the intra-gravel flow (with a relatively low dye concentration) is enhanced in the region of the redd. The activated charcoal detector technique has shown promise for future experiments involving tracers below the bed. A separate study, perhaps involving different tracer or detector

materials, might well be able to significantly improve it, or perhaps extend it to fieldwork.

4.3 SIDO-UK Model

In order to make the model more realistic it would be possible to implement the flow and intragravel flow model within a three-dimensional grid using the near-bed flow as the boundary conditions. The intragravel flow-through cells could be defined with respect to whether the flow through them is Darcian or turbulent, potentially yielding more accurate flow rates and hence oxygen fluxes. Reconfiguring the intragravel component alone would be relatively simple, but this could create problems in justifying the accuracy of the output given unsophisticated boundary conditions. More significant for immediate practical application is the need for quality data defining the impact on egg survival of sedimentation and, more especially, predictive functions determining fry emergence.

With provisos noted below the SIDO-UK model results produce predictive values and trends which indicate that the hydraulic regime in a northern UK upland river provides only a fragile habitat for salmonids. This supposition is supported by the evidence of a reduction in the numbers of spawning salmonids in rivers such as the Lune in recent years. The model demonstrates that the reduction in recruitment could reasonably be atrributed to increased intensity of floods and suspended sediment events due to climatic change, or due to some other more direct anthropogenic disturbance to the ecosystem. However, the observed sensitivity of the oxygen concentrations modelled by SIDO to the composition of the redd gravel, the coefficient CBADJ, and the mean velocity of the flow above the redd, suggest that well-focussed study is needed of selected field sites, as is discussed below.

In conclusion, it would appear that the SIDO model can be applied to the UK situation, but as with all physico-biological models of complex systems, its predictions are effected by the cumulative effect of uncertainties associated with a number of factors which remain poorly parameterized.

4.4 Suggestions for Future SIDO-UK Development

At this juncture it may be concluded that SIDO-UK may be used with care to demonstrate the likely improvement or decline in environmental conditions and recruitment of fish. For a truly predictive quantitative capability further work is required not only in modifying parameters using information in the literature, but also in developing specific studies which will produce better parameterization. Many of the existing algorithms can be adapted for the UK situation, but there are some inconsistencies which require further investigation. For example, the model still utilises functions for fry emergence that pertain to North American species. These latter functions indicate a non-zero value for fry emergence even when the eggs have been starved of oxygen. This aside, the predicted flow velocities, oxygen concentrations and times to hatching for what is an extremely complex situation to model appear to be consistent with observations.

Future work would benefit from the following physical data:

- Measurements and calibration information pertaining to one or more particular site(s) of national importance, studied over at least one spawning season, including direct measurements of rates of sediment in-filling of redds in order to properly calibrate the coefficient CBADJ in the model, and direct measurements of suspended sediment loads.
- A more detailed set of cross sections corresponding to a pool/riffle sequence, so that the redd can be located near the entry to a riffle section.

Future work would benefit from the following biological data:

- A definative study of the physiology of developing salmonid fish eggs not only as isolates but also in more natural clumped groupings where there is competition for oxygen supply and metabolic waste removal.
- Better information on the effect of multiple factors, such as DO concentration, temperature and intragravel flow rate acting together on time to egg maturation.
- Improved understanding of the controls on recruitment at the time of fry emergence.

If this information were available the assumptions that are made in the different sub-algorithms of SIDO could be more thoroughly tested.

5 CONCLUSIONS

In conclusion it is evident that a 3-D representation of a salmonid redd gives a more realistic impression of the flow field than simple 2-D models. Mapping of detailed turbulence parameters shows graphically and conclusively the detail of the flows interaction with the redd morphology and importantly explains the role of this flow field in driving a strong intragravel flow through the critical part of the redd wherein egg pockets are to be found. The main intragravel flow lines can be traced and it has been shown that the rate of flow (demonstrated by dye absorption) is greatest in the vicinity of egg pockets.

The SIDO-UK model results demonstrate that salmonid redds are very susceptible to siltation in-as-much as recruitment is adversely effected. Thus the flow and sediment regime in a northern UK river, such as the Lune, provides a fragile habitat for salmonids. There is some uncertainty as to the degree of impact predicted by SIDO-UK, yet it is evident that the reduction in the numbers of spawning salmonids on rivers such as the Lune in recent years, could be as a result of increased frequency and severity of floods and higher suspended sediment loads. These changes may be due to climatic change, or due to anthropogenic disturbance within the catchments. Despite some current limitations and the uncertainties in prediction, SIDO-UK is a potentially valuable tool for monitoring and managing UK salmonid rivers. However, the observed sensitivity of the oxygen concentrations modelled by SIDO-UK to the composition of the redd material, the coefficient CBADJ, and the mean velocity of the flow above the redd, indicates that more carefully focussed studies need to be carried out, to determine salmonid requirements, as is suggested below.

In conclusion, it would appear that the SIDO-UK model can be applied to the UK salmonid rivers, but as with all physico-biological models of complex systems, it suffers from the cumulative effect of uncertainties from a large number of parameters becoming propagated into large uncertainties in the predictions.

In the light of this short piece of research, the application of SIDO to UK situation requires some more work. It would appear that although many of the algorithms can be adapted for the UK situation, there are some inconsistencies which require further investigation, such as the failure of the model to predict that the percentage fry emergence must surely drop to zero, if the eggs have been starved of oxygen. This aside, the predicted flow velocities, oxygen concentrations and times to hatching for what is an extremely complex situation to model appear to be consistent with observations.

Future work would benefit from the following:

1) Measurements and calibration information pertaining to one particular site, studied over at least one spawning season, including direct measurements of rates of in-filling of redds in order to properly calibrate the coefficient CBADJ in the model, and direct measurements of suspended sediment loads.
2) A more detailed set of cross sections corresponding to a pool/riffle sequence, so that the redd can be located near the entry to a riffle section.

If this amount of information could be ascertained for one particular site, the large number of assumptions that are made in the different sub-algorithms of SIDO could be more thoroughly tested.

6 REFERENCES

Acornley, R.M., (1999) 'Water temperatures within spawning beds in two chalk streams and implications for salmonid egg development', Hydrological Processes, 13, 439-446.

Acornley, R.M. and Sear, D.A., (1999) "Sediment transport and siltation of brown trout (*Salmo trutta L.*) spawning gravels in chalk streams", Hydrological Processes 13, 447-458.

Alonso, C.V., Theurer, F.D. & Zachmann, D.W. (1996) "Tucannon River Offsite Report: Sediment Intrusion and Dissolved Oxygen Transport Model", Technical Report No.5, USDA National Sedimentation Laboratory.

Bennett, S.J. & Best, J.L. (1995) "Mean flow and turbulence structure over fixed, two dimensional dunes: implications for sediment transport and bedform stability", Sedimentology, 42, 491-513.

Blaxter, J.H.S., 1969, "Development: eggs and larvae", Chapt. 4 in 'Fish Physiology', Ed. W.S.Hoar and D.J. Randall. Vol.3. Academic Press, London 486pp.

Burner, C.J. (1951) Characteristics of spawning nests of Columbia River salmon. U.S. Fish and Wildlife Service Bulletin, 61, 97-110.

Carling, P.A. (1984a) "Deposition of fine and coarse sand in an open-work gravel bed", Canadian Journal of Fisheries and Aquatic Sciences, 41, 263-270.

Carling, P.A., (1984b) "Comparison of suspended sediment rating curves obtained using two sampling methods' in 'Channel Processes – water, sediment, catchment controls", A.P. Schick (Editor), CATENA supplement 5, Braunschweig.

Carling, P.A., (1985) "Oxygen flux through salmonid spawning grounds", Freshwater Biological Association, Project 73 Report.

Carling, P.A. and McCahon, P. (1985) Natural siltation of brown trout *(Salmo Trutta L.)* spawning gravels during low flow conditions, In: 'Regulated streams Advances in ecology', J.F. Craig and J. Bryan Kemper (Editors), Plenum Press, NY.

Chapman, D.W. (1988) "Critical review of variables used to define effects of fines in redds of large salmonids", Transactions of the American Fisheries Society, 117, 1-21.

Cooper, A.C. (1965) "The effect of transported stream sediments on the survival of sockeye and pink salmon eggs and alevins". Int. Pac. Salmon Fish. Comm. Bulletin 18, 71pp.

Crisp, D.T, (1981) "A desktop study of the relationship between temperature and hatching time for the eggs of five species of salmonid fishes", Freshwater Biology, 11, 361-368.

Crisp, D.T., (1990) "Water temperature in a stream grave bed and implications for samonid incubation", Freshwater Biology, 23, 601-612.

Crisp, D.T. & Carling, P.A. (1989) "Observations on siting, dimensions and structure of salmonid redds", Journal of Fish Biology , 34, 119-134.

Daykin, P.N. (1965) "Application of mass transfer theory to the problem of respiration of fish eggs", J. Fisheries Board Of Canada, 22,159-171.

DeVries, P. (1997) "Riverine salmonid egg burial depths: review of published data and implications for scour studies", Canadian Journal of Fisheries and Aquatic Sciences, 54, 1685-1698.

Elliot, J.M., (1984) "Numerical changes and population regulation in young migratory trout *Salmo Trutta* in a Lake District stream", 1966-1983', J. Animal Ecology, 53, 327-350.

Elliot, J.M. and Hurley, M.A., (1998) "An individual-based model for predicting the emergence period of sea trout fry in a Lake District Stream", J. Fish Biol., 53, 414-433.

Everest, F.L., Beschta, R.L., Scrivener, J.C., Koski, K.V., Sedell, J.R. & C.J. Cederholm.(1987) "Fine sediment and salmonid production - a paradox", In: Streamside Management: Forestry and Fishery Interactions, E.O. Salo & T.W. Cundy (Editors).

Freshwater and Salmon Fisheries Research (1960) "The Fecundity of Atlantic Salmon', Publ. Pickering and Inglis Ltd".

Grost, R.T., Hubert, W.A. & Wesche, T.A. (1991) "Description of brown trout redds in a mountain stream" Transactions of the American Fisheries Society,120, 582-588.

Hamor, T. and Garside, T., (1976) "Developmental rates of embryos of Atlantic salmon, *Salmo salar L*., in response to various levels of temperature, dissolved oxygen, and water exchange", Can. J. Zool., 54, 1912-1917.

Harrison, S.S. and Clayton, L. (1970) Effects of groundwater seepage on fluvial processes. Geol. Soc. Am. Bull., 81, 1217-1226.

Helle, J.H.(1970) "Biological characteristics of intertidal and freshwater spawning of pink salmon at Olsen Creek, Prince William Sound, Alaska, 1962-1963", Special Scientific Report on Fisheries 602.

Hobbs, D.F. (1937) Natural reproduction of Quinnat Salmon , Brown Trout in certain New Zealand waters. N.Z. Marine Department of Fisheries Bulletin No. 6.

Humpesch, U.H. (1985) "Inter-specific and intra-specific variation in hatching success and embryonic-development of 5 species of Salmonids and Thymallus-thymallus" Archiv für Hydrobiolgie, 104, 129-144.

Kondolf, G.M. (1988) "Salmonid spawning gravels: A geomorphic perspective on their size distribution, modification by spawning fish, and criteria for gravel quality" Unpublished Ph.D. thesis, John Hopkins University, Baltimore, USA.

Kondolf, G.M., Sale, M.J. & Wolman, M.G. (1993) "Modification of Fluvial Gravel Size by Spawning Salmonids", Water Resources Research, 29, 2265-2274.

Kondolf, G.M. & Wolman, M.G. (1993) "The sizes of salmonid spawning gravels", Water Resources Research, 29, 2275-2285.

McNeil, W.J. & Ahnell, W.H. (1964) "Success of Pink Salmon spawning relative to size of spawning bed materials", Spec. Sci. Rep. Fish (469), 15pp.

Orr, H.G.,(1996) "Geomorphological change of River Lune" Unpublished M.Phil. Thesis, Lancaster University, UK.

Ottaway, E.M., Carling, P.A., Clarke, A. & Reader, N.A. (1981) "Observations on the struc-ture of brown trout, Salmo trutta Linnaeus, redds", J. Fish Biol., 19, 593-607.

Page, B. (1998) "The morphological response of the River Lune to being straightened and diverted between Gaisgill and Newbiggin on Lune" Unpublished Dissertation, Lancaster University, UK.

Porter. P. (1985) "Comparison between the subsurface environment of brown trout redds and non redd sites in two North Carolina streams" MS Thesis.

Ringler, N.H. (1970) "Effects of logging on the spawning bed environment in two Oregon coastal streams" MS thesis, Oregon State University, USA.

Simons, D.B. and Senturk, F., (1977) "Sediment transport technology", Water Resources Publications, Fort Collins, Colorado, 80522, USA.

Stuart, T.A. (1953) Spawning migration, reproduction, and young stages of loch trout (*Salmo trutta L.*), Freshwater and Salmon Fisheries Research No. 5, Scottish Home Department, Edinburgh, UK.

Taylor, P. (2000) 'Turbulent Flow Above Salmonid Redd' Unpublished M.Phil thesis, Lancaster University, UK.

Theurer, F.D. (1985) "Evaluating impacts of soil and water conservation measures" Proceedings, Natural Resources Modelling Symposium, 1-6.

Theurer, F.D. and Miller, W.J., (1986) "Tucannon River offsite study: fry emergence model report", USDA-ARS Hydro-Ecosystem Research Unit, Ft. Collins, CO.

Thibodeaux, L.J. & Boyle, J.D. (1987) "Bedform generated convective transport in bot-tom sediment", Nature, 325, 341-343.

Thurow, R. & King, J. (1990) "Effects of Fine Sediment on Fish Populations", Pages 11-49 to 11-56 in Shou-Shan Fan and Yung-Huang Kuo (Editors) Proceedings of the Fifth Federal Interagency Sedimentation onference, 2,March 1991, Las Vegas, Nevada, USA.

Wickett, W.P. ,(1975) "Mass transfer theory and the culture of fish eggs", In: ‘Chemistry and physics of aqueous gas solutions", W.A. Adams (Editor), The Electrochemical Society, Princeton, 521pp.

7 APPENDIX

The equations and figure numbers that are not referenced pertain to the SIDO manual (Alonso et al., 1996). There are additional changes that have to made to define the River reach cross-sectional geometry, not shown here. There are also mixed units in the table because of the American / UK unit discrepancy, although *the model has been adjusted such that data is input in metric units.* Changes relevant to the UK situation are given in column 4 in brief, but are discussed further in the main text.

Table 7.1 of all parameters to be varied for British species (Atlantic salmon and brown trout) and northern UK conditions

File and Parameter used in SIDO model	**Description**	**Example values for Tucannon river and Chinook / Steelhead** (used in the SIDO manual)	**Values changed to for River Lune and Atlantic salmon / trout**	**Reference / comments**
Jobcntrl.inp	**Options for model type**			
JSTART	Fertilisation data	1.	1	Variable Choice
NDAYS	No. days of cycle	-	180	"
CHINOOK	Flags Chinook properties or Steelhead properties	TRUE FALSE	Atlantic salmon Brown trout	Changed to represent UK situation
Hydrolog.inp	***Hydrology data***			
QD	Day dependent Q	Uses time series	Daily time series for Lune	Environment Agency data
TEMP	Daily temperature	Data of order (~) 10 C	Mean of 8 C Monthly means from E.A data	E.A. data and Crisp (1990)
FSLD1	Q dependent clay (ppm)	~60 ppm (p3-15)	Zero	
FSLD2	Q dependent silt (ppm)	~270 ppm	SS rating curve corrected for near – bed, see main text. silt fraction only.	Carling (1984) Carling and McCahon (1985)
FSLD3	Q dependent sand (ppm)	~30 ppm	Zero	
Strmredd.inp	Redd information			
S0_below	Bed slope below redd	0.0055	0.0064	Page, B (1998)
Num_X_sec	Number of river X sections	Any number	2	Page, B (1998)
Q_bedload	Gravel substrate set in motion – run terminated (i.e. redd obliterated)	10000 ft^2/s = 930 m^2/s	Unchanged. Only occurs in most catastrophic events.	Alonso et al. (1995)

Q_calb	Discharge for Manning's n calibration	~2 cumecs	5.4 cumecs (this is used to determine V from Q=VA, and V will then be used in eq1-4	Orr, H (1996)
N_calb_exp	Exponent of total conveyance relationship Eq.1-12 factor beta	0.3	0.3	P1-22 leave unchanged – based on US and UK studies
X0RDD	Distance between downstream of redd and downstream X section	Any	~50m	Page, B (1998)
RELEV	Above sea level	Any	182 m	Orr, H (1996)
CROSS SECTION	**Cross section 1 is furthest downstream**			
X_long	X location upstream	Any	200m	Page, B (1998)
Num_pnts	16,19		16,19	Page, B (1998)
Bankfull	When overbank flow occurs		8.0,8.5m	Page, B (1998)
D50_bed	Characteristic bed material size – for bed load transport	For each cross section e.g. 60mm used in equ 1-9	56mm average in riffle section	Orr, H (1996)
Dn_rough	As above for channel bed roughness	60mm	56mm assumed the same as above measure	Orr, H (1996)
N_ovrbnk	Manning for overbank region	0.050	0.05 is typical value used	
N_calb	Calibrated mannings n for in channel flow Value obtained by fitting the stage profile. Can be determined from field data using expression for n' in eqn 1-9. This needs D50 and R (dependent on Q and cross section info) only and is based on some UK rivers (as well as other countries)	0.033	0.025 Estimated from D_{50} using standard formula: $n=aD_{50}^{b}$ where a=0.04, b=1/6. Calibrated water surface slope data not available.	

BLKDAT.FOR ALL PARAMETERS THAT MAY BE AFFECTED BY CHANGE OF FISH	Internally set information			
Eggs				
NBEGGS	No laid per female	3900 / 4000	Brown trout: dependent on female size :for Black Brows beck $Y=aX^b$ X=45.5cm, a=0.72, b=2.04 Y=1737 Or in 98 with more data: X=455mm, a=0.0063, b=2.05 Y=1771 Atlantic Salmon: for 55cm length (shortest available) mean egg count per female of 2525. Using regression for 45 cm fish: 1585	Elliot (1984) Elliot and Hurley (1998) Freshwater and Salmon Fisheries research (1960)
RADIUS	Egg radius	0.42 cm / 0.32 cm	Cross sectional area=$0.157cm^2=\pi r^2$ R_{trout} =0.22cm Dsalmon=5.6mm R=0.28cm	Wicket (1975) for Brown Trout FSF (1960)
THICK	Egg capsule thickness	0.008 / 0.0035 cm	0.008 / 0.0035	
VEGGZN	Vol of redd egg zone	255 litres / 191 liters	Seems too big for UK – under investigation **: approximately 100 l (length*depth*width) of egg zone (1.11*0.14*1.0=0.15 $5m^3$) =155l Elliot: (0.65*0.6*0.18=70l	Crisp and Carling (1980) Elliot (1984)
CE	O2 conc within egg capsule for chin/sthd	0.002 / 0.002mg/cc	0.0025 mg/cc	Blaxter (1969)
DC	Diffusion coefficient through egg capsule	$0.18*10^{-5}$ cm2/s	Unchanged - Only data available $1.26*10^{-5}$ in Wickett (1954) $0.72*10^{-9}$ * TEMP (K)/$1.308*10^{-2}$ = $1.56*10^{-5}$ for 283K or for 281K (Carl beck) : 1.55	Daykin (1965)

Sediment				
DEOXYK	Dimensionless deoxygenation const	0.0471	0.0471	Unchanged – fixed parameter
DOEXP	Correction factor			"
SEDSOC	O2 consump	11.38mg of o2 per g silt	Unchanged – appropriate for UK also	Carling (pers. comm)
TMPREF	Ref temp. for sediment O_2 concentration	20 C	20 C	Unchanged
Routing parameters				
BTCHNK / BTSTHD	BETA in fig1-19 p1-34 or in Crisp and Carling: approximately (atan((f+e)/ (p/2+q/2)) where f=k-h	12 / 14	Average female length in NE England sample of trout and salmon combined was 45.5cm. ln(redd tail length)=b×ln(fish length) +lna where lna=0.45, b=1.18 average redd tail length =142cm (both species) ln(pot length)=b×ln(tail length) +lna where lna=0.46, b=0.80 average pot length = 81cm L=(81+142)/2=111cm D_{both} = 14.2cm BETA ≈ atan (2D/L) $BETA_{b.trout}$=atan(28.4/111) =14.3	FIG 1-19 Information and regressions from Crisp and Carling (1989) Depths of egg burial are for b.trout and Salmon in NE England. Lengths (pits and tails) for mean fish length from sample of trout and salmon in NE England.
ZETA	Dimensionless depth used in comparing concentration of ss fines near stream redd interface	0.05	Unchanged	P3-8
DXCHNK / STHD DYCHNK / STHD	Width and height of finite difference cells	0.5ft/0.375ft 0.125ft /0.125 ft (unchanged)	These have been reduced for better resolution	P3-8
NODEID	Identifiers for cells pertaining to each redd subdomain – each fd cell is assigned class 1-4 for 4 zones	P 3-8 figure	Unchanged: these represent flags for substrate material composition. The manual uses a single set for both species, despite different redd dimensions. Since the average redd is similar for UK average fish size, use the same subdomains.	

Redsite.inp	Inter gravel transport parameters			
Alpha	Loss of water through bed	0.	0 – negligible	No loss/gain
CPERM	Controls hydraulic conductivity in clean partially filled gravel. Need to ensure that intra-gravel flow sweeps the clean portion of the redd in a time not much > 1day. (compute the average intra-gravel flow travel time over the length of the redd	92.(unchanged)	Unchanged – appropriate for UK	
CBADJ	Coefficient Multiplying near bed suspended sediment conc.: should be adjusted such that the redd fills up within the either the observed or expected time span	50 First layer is filling over 16 days for given s.s. loads	This coefficient was left between 1-50 for the different scenarios. The correction using Rouse's equation was implemented for the near bed suspended sediment load, as there was no on-site information for the rate of filling. McCahon do give some rates of filling, which could be investigated further, but these need to be used in conjunction with the corresponding hydrograph and bed form.	Carling and McCahon, (1985) Northern England upland river.
VSADJ	Controls rate of sed settling (0-1). 1 adequate for most circs	1.0 left at this value	Unchanged	P3-7
BSWFNS	Bulk specific weight of substrate material	80	Unchanged	P3-7
BSWGRV	As above	110	Unchanged	
	Grain size diameter of sediment fractions (mm)		Unchanged – these are pertinent to UK	Carling (pers. comm)
DGS1		0.002		
DGS2		0.061		
DGS3		0.106		
DGS4		0.85		
DGS5		2.00		
DGS6		6.35		
DGS7		9.50		
DGS8		25.40		
DGS9		50.80		
DGS10		100.0		

	Specific gravity of sediment fractions		Unchanged – these are pertinent to UK	Carling (pers. comm)
SGG1		2.00	"	
SGG2		2.20	"	
SGG3		2.65	"	
SGG4		2.65	"	
SGG5		2.65	"	
SGG6		2.65	"	
SGG7		2.65	"	
SGG8		2.65	"	
SGG9		2.65	"	
SGG10		2.65	"	
	Initial size composition of substrate material for three zones (undisturbed, disturbed and egg zones)			
PCF1		0.00 0.00 0.00	0.00 0.00 0.00	Unchanged
PCF2		0.00 0.00 0.00	0.00 0.00 0.00	Unchanged
PCF3		0.00 0.00 0.00	0.00 0.00 0.00	Unchanged
PCF4		0.01 0.01 0.01	0.10 0.10 0.10	Crisp and Carling (1989) linear Interpolation Between 1mm (10% finer) and 56mm (50% finer) Y=0.73x+9.27
PCF5		0.09 0.09 0.09	0.11 0.11 0.11	
PCF6		0.45 0.45 0.45	0.14 0.14 0.14	
PCF7		0.95 0.95 0.95	0.16 0.16 0.16 – these had to be set to 0.25 or else insufficient coarse material to define blocked cells around pit	
PCF8		1.00 1.00 1.0	0.28 0.28 0.28	
PCF9		1.00 1.00 1.0	0.46 0.46 0.46	Orr (1996)
PCF10		1.00 1.00 1.0	1.00 1.00 1.00	Unchanged
BSWMIX		130. 110. 110.	130. 110. 110.	Unchanged
	COMPOSITION OF BED MATERIAL THAT FILLS THE REDD'S DEPRESSION DURING BEDLOAD MOVEMENT (mass fraction finer than, in decimal) zone 4 - bedload			
PCFILL1		0.00	0.00	Same as new substrate above
PCFILL2		0.00	0.00	
PCFILL3		0.00	0.00	
PCFILL4		0.00	0.00	
PCFILL5		0.00	0.10	
PCFILL6		0.060	0.11	
PCFILL7		0.10	0.14	
PCFILL8		1.00	0.25	
PCFILL9		1.00	0.28	
PCFILL10		1.00	0.46	
BSWMIX		110.	110	